PCCP

Accepted Manuscript

ROYAL SOCIETY OF CHEMISTRY

www.rsc.org/pccp

An Accurate Benchmark Description of the Interactions between Carbon Dioxide and Polyheterocyclic Aromatic Compounds Containing Nitrogen

Sicheng Li, Daniel G. A. Smith, and Konrad Patkowski*

Department of Chemistry and Biochemistry, Auburn University, Auburn, AL 36849, *United States*

(Dated: May 22, 2015)

Abstract

We assessed the performance of a large variety of modern density functional theory approaches for the adsorption of carbon dioxide on molecular models of pyridinic N-doped graphene. Specifically, we selected eight polyheterocyclic aromatic compounds ranging from pyridine and pyrazine to 1,6-diazacoronene and investigated their complexes with CO_2 for a large range of intermolecular distances and including both in-plane and stacked orientations. The benchmark interaction energies were computed at the complete-basis-set limit MP2 level plus a CCSD(T) coupled-cluster correction in a moderate but carefully selected basis set. Using a set of 96 benchmark CCSD(T)-level interaction energies as a reference, we investigated the accuracy of DFT-based approaches as a function of the density functional, the dispersion correction, the basis set, and the counterpoise correction or lack thereof. While virtually all DFT variants exhibit some deterioration of accuracy for distances slightly shorter than the van der Waals minima, we were able to identify several schemes such as B2PLYP-D3 and M05-2X-D3 whose average errors on the entire benchmark data set are in the 5–10% range. The top DFT performers were subsequently used to investigate the energy profile for a carbon dioxide transition through model N-doped graphene pores. All investigated methods confirmed that the largest, N4H4 pore allows for a barrierless CO_2 transition to the other side of a graphene sheet.

* Corresponding author, email: patkowsk@auburn.edu

I. INTRODUCTION

Novel carbon-based nanomaterials such as graphene and carbon nanotubes exhibit a wide range of mechanical and electronic properties and have been proposed for a variety of applications. Even more diversity, in particular, both n-type and p-type semiconductor character, can be introduced by doping pristine nanostructures with heteroatoms such as nitrogen, boron, or oxygen. The nitrogen-doped structures, the subject of this work, are of particular importance. The microscopic structure of N-doped carbon nanotubes has been studied using both experiment and molecular simulations [1–6] and two local patterns around dopant atoms have emerged. The first one, the "graphitic" structure, involves a simple substitution of a nitrogen atom in place of one of the carbon atoms. This structure involves an unpaired electron that ends up on a delocalized $\pi^\star$ state [4, 7]. The second, "pyridine-like" pattern, which will be the focus of the present study, involves 2–4 sp^2 nitrogen atoms in pyridinic rings surrounding a vacancy. The three-nitrogen vacancy is a particularly popular model and the presence of such vacancies has been confirmed by scanning tunneling microscopy [1]. Slightly larger vacancies are interesting as potential "holes" for small molecules to enter and exit the nanotubes or to pass through a porous graphene membrane [8–20].

Noncovalent interactions of graphene and carbon nanotubes with adsorbed molecules are of broad significance [21] due to the proposed applications of nanotubes in chemical sensing [22] and gas storage and separation [23] as well as the possibilities of tuning nanotube properties via noncovalent functionalization [24]. In particular, the separation of carbon dioxide from flue and exhaust gases through selective adsorption is one of the most promising ways to reduce global carbon emissions, and carbon-nanotube based materials, while not as effective as the most recent generations of metal organic frameworks [25], provide a viable medium for CO_2 sequestration [26]. It should be noted that the interaction of carbon nanotubes (pristine or doped) with CO_2 and other adsorbed small molecules is dominated by dispersion and thus provides a difficult target for *ab initio* computational chemistry, most notably for methods based on density functional theory (DFT). A wide variety of new methods have been devised to overcome the inherent inability of DFT to account for long-range correlation [27–34] and these new methods provide enormous improvement over standard generalized gradient approximation (GGA) or hybrid functionals when it comes to noncovalent interaction energies. As averaged over popular databases of weak interaction energies [35–37],

the novel DFT variants have long surpassed chemical accuracy (1 kcal/mol) in the van der Waals minimum region, reaching well into the 0.2–0.3 kcal/mol range [38]. However, this accuracy, which corresponds to a relative accuracy of about 10% for the systems considered here, is by no means consistent across either different systems or different intermolecular separations, and one has to select an optimal DFT variant on a case-by-case basis, through careful benchmarking against accurate wavefunction-based interaction energies for relevant models. We have previously performed such benchmarking and functional selection for models of graphene and pristine carbon nanotubes interacting with methane [39, 40] and carbon dioxide [41].

For the interaction of a CO_2 molecule with N-doped graphene and carbon nanotubes, a natural class of models are dimers of CO_2 with nitrogen-containing polyheterocyclic aromatic compounds (N-PHACs) containing one or more pyridinic nitrogen atoms. Such dimers, along with similar 1- and 2-ring complexes (involving, e.g., the purine molecule) were the subject of a high-level (up to the supermolecular coupled-cluster method with single, double, and perturbative triple excitations, CCSD(T)) computational study of Vogiatzis *et al.* [42]. These authors identified the global-minimum structures for 13 N-PHAC–CO_2 dimers and obtained benchmark interaction energies close to the CCSD(T) complete basis set (CBS) limit. The study of Ref. 42 was later employed by Mackie and DiLabio [43] as a benchmark for their DFT-based study of the CO_2 adsorption on N-doped carbon nanotubes. However, none of the models considered in Ref. 42 had more than two aromatic rings, while our methane adsorption study [39] indicated that the one- and two-ring aromatic fragments provide quite poor models of extended carbon nanostructures.

In this paper, we attempt to find the best-performing DFT variant for the CO_2 adsorption on graphene and carbon nanotubes N-doped into a pyridinic structure. To this end, we first select a set of sixteen benchmark N-PHAC–CO_2 structures that cover both the global-minimum, planar geometries and the three-dimensional stacked structures. The N-PHACs present in the benchmark set range from one ring (pyridine, pyrazine) to seven rings (1,6-diazacoronene). The coronene-sized models are the largest ones for which reliable benchmark interaction energies, accurate to below 0.1 kcal/mol at the van der Waals minima, can be obtained using the composite MP2/CBS+ΔCCSD(T) (CBS-extrapolated second-order Møller-Plesset perturbation theory plus a CCSD(T) correction in a moderately sized basis set) approach [39, 40]. Alternatively, one could use some approximate,

local coupled-cluster methods [44–47] but we have not pursued this approach here as it is not clear how the associated approximations affect the uncertainty of the benchmark. We consider six different intermolecular separations along a one-dimensional cut through the potential energy surface (PES) for each structure, resulting in 96 data points for which benchmark MP2/CBS+ΔCCSD(T) interaction energies are computed. A variety of DFT functionals with different atom-pairwise dispersion corrections and basis sets are then compared to this benchmark in order to find a top performer. This top performer is then used to obtain CO_2 adsorption energies on larger N-PHAC models, in particular, to model the barrier to the CO_2 transition through three different vacancies in an N-doped graphene sheet.

II. METHODS AND COMPUTATIONAL DETAILS

The MOLPRO [48] program was used to obtain all conventional and explicitly correlated MP2 and CCSD(T) interaction energies. The MP2 calculations employed density fitting (DF-) [49] and used standard orbital and auxiliary bases aug-cc-pVXZ≡aXZ [50, 51] and aug-cc-pVXZ/MP2FIT [52, 53], respectively. To keep the errors of the DF approximation under control, we needed to resort to conventional, non-density-fitted Hartree-Fock calculations in the aDZ and aTZ bases. Moreover, for the explicitly correlated MP2 (MP2-F12) calculations, the `df-basis-exch` and `ri-basis` auxiliary bases were chosen as the aug-cc-pVXZ/JKFIT sets instead of the MOLPRO default non-augmented sets. We found that this change in auxiliary bases was critical for the accuracy of MP2-F12 but had a negligible effect on the ΔCCSD(T) term so we kept the default auxiliary bases in the ΔCCSD(T)-F12 calculations. As the cost of DF-MP2 is just a small fraction of that of conventional MP2, only DF-MP2 calculations are feasible in the aQZ and a5Z bases for larger N-PHACs. The "DF-" qualifier will be dropped from now on. Unless noted otherwise, all computations utilized the counterpoise (CP) correction for the basis set superposition error (BSSE) [54, 55]. The 1s carbon, nitrogen, and oxygen electrons were not correlated.

A. Geometries of the Model Complexes

To obtain the lowest-energy geometry for each dimer, first, a geometry optimization for all N-PHAC and CO_2 monomers was performed at the MP2/aTZ level. The dimer was then optimized at the MP2/aTZ level with only the intermolecular degrees of freedom allowed (in other words, the intramolecular degrees of freedom were frozen). In order to consider different modes of interaction between CO_2 and N-PHACs, two arrangements, one with CO_2 stacked over the N-PHAC surface and parallel to it, and the other with the CO_2 carbon in the same plane as the N-PHAC, are taken into consideration. The parallelity of the CO_2 molecule to the N-PHAC plane (stacked structures) as well as the maximum point-group symmetry were forced during the optimization, but the intermolecular distance and the angles that do not affect symmetry and parallelity were freely optimized. The global minimum position for all complexes occurs when the CO_2 carbon lies in the N-PHAC plane. In addition to the minimum geometries, we computed interaction energies along radial cross sections through the potential energy surfaces passing through the minimum and lowest-energy stacked geometries. In other words, we shifted the distance z between the monomers with all the angles fixed relative to the line connecting the monomers. The values of z given throughout the rest of the text are the distances between the CO_2 carbon and the closest nitrogen for the in-plane dimers (except phenanthroline-CO_2, where the z value is the distance from the CO_2 carbon to the midpoint between the two closest carbon atoms in the middle ring of phenanthroline). For all the stacked geometries, the z values are the distances between the CO_2 carbon and the N-PHAC plane. The lowest-energy in-plane and stacked geometries for each dimer are displayed in Fig. 1. The stacked configuration was picked to be parallel since all resulting geometries have at least C_s symmetry, lowering the overall computational cost compared to other possible stacked structures. The only exception is the quinoline-CO_2 complex for which, as shown in Fig. 1, the stacked configuration cannot have C_s symmetry. However, we still forced the CO_2 molecule to be parallel to the quinoline plane to get a consistent set of sixteen geometries.

B. Benchmark Energies from Wave-Function Methods

Following the standard practice in the field [56], the benchmark interaction energy is computed as

$$E_{\rm int}^{\rm benchmark} = E_{\rm int}^{\rm MP2}/({\rm a}(X{\rm –}1){\rm Z},\, {\rm a}X{\rm Z}) + \Delta E_{\rm int}^{\rm CCSD(T)}/({\rm a}(X'{\rm –}1){\rm Z},\, {\rm a}X'{\rm Z}), \quad (1)$$

where $E_{\rm int}^X = E_{\rm AB}^X - E_{\rm A}^X - E_{\rm B}^X$ is the supermolecular interaction energy at a given level of theory, $\Delta E_{\rm int}^{\rm CCSD(T)} = E_{\rm int}^{\rm CCSD(T)} - E_{\rm int}^{\rm MP2}$ is the CCSD(T) contribution missing at the MP2 level, and the notation (basis1, basis2) represents that the bases "basis1" and "basis2" have been utilized in the standard X^{-3} extrapolation for the correlation part of the interaction energy [57]. The X^{-3} extrapolation has been employed for both the conventional and explicitly correlated MP2 and CCSD(T) contributions [58, 59]. The self-consistent field (SCF) part of the interaction energy was taken from the calculation employing the larger of the two bases and not extrapolated. The notation ΔCCSD(T)/aXZ indicates a correction that is calculated in the aXZ basis set without extrapolation. Moreover, MP2/$(X-1, X)$ and ΔCCSD(T)/$(X-1,\ X)$ will be the short-hand notations for $E_{\rm int}^{\rm MP2}$/(aug-cc-pV$(X-1)$Z, aug-cc-pVXZ) and $\Delta E_{\rm int}^{\rm CCSD(T)}$/(aug-cc-pV$(X-1)$Z, aug-cc-pV$X$Z), respectively.

To investigate the basis set convergence of the ΔCCSD(T) contribution, explicitly correlated CCSD(T)-F12 calculations were performed for seven 1-ring and 2-ring dimers (except for the C_1 stacked quinoline-CO_2 complex). The CCSD(T)-F12a and CCSD(T)-F12b approximations [60, 61] use the default MOLPRO [48] values for the explicitly correlated *Ansätze*, geminal parameters, and auxiliary bases. Since the triples contributions to CCSD(T)-F12a and CCSD(T)-F12b do not include explicit correlation (an explicitly correlated (T) correction has been derived [62] but exhibits a steeper computational scaling), we employed the popular estimate of the missing F12 contributions to $\Delta E^{\rm (T)} = E^{\rm CCSD(T)-F12} - E^{\rm CCSD-F12}$ via scaling:

$$\Delta E^{\rm (T**)} = \Delta E^{\rm (T)} \cdot \frac{E_{\rm corr}^{\rm MP2-F12}}{E_{\rm corr}^{\rm MP2}}, \quad (2)$$

where the subscript "corr" represents the correlation energy at a given level of theory. To ensure size consistency, the scaling factor calculated for the dimer was also employed in the counterpoise-corrected calculations for the monomers [63]. Throughout this work, the notations "(T)" and "(T**)" will refer to the unscaled and scaled triples corrections

in CCSD(T)-F12, respectively. The CCSD(T)-F12 approach in its various approximate variants provides greatly improved weak interaction energies in double- and triple-ζ basis sets compared to conventional CCSD(T) results [63–65].

C. DFT Calculations

Among the many new variants of DFT that include some form of dispersion, the three groups tested in this work are the functionals specifically optimized for benchmark weak interaction energies, the DFT+D approaches with an atom-pairwise dispersion correction added on top of a standard density-functional calculation, and the double hybrid DFT functionals. In this work, we examined a few representative members of each group. For the first group, the interaction-optimized functionals, we included M05-2X [66] and M06-2X [29]. Among the second group, DFT+D, we employed the widely popular B3LYP [67, 68], BLYP [69], BP86 [69], PBE [70], PBE0 [71, 72], and LC-ωPBE [73] methods as well as Grimme's reparameterization [27] of Becke's B97 functional [55]. These five functionals were augmented by Grimme's atom-pairwise dispersion terms in the -D2 [27], -D3 [33], -D3(BJ) [74], -D3-$E^{(3)}$, and -D3(BJ)-$E^{(3)}$ variants. For the last group, we tested the B2PLYP [75] double hybrid functional.

All DFT interaction energies except for B2PLYP and LC-ωPBE were calculated using MOLPRO 2012.1 [48] locally modified to include Grimme's reparameterization of B97. The requested energy convergence threshold for MOLPRO calculations was at least 10^{-7} hartree (10^{-8} for the M05-2X and M06-2X functionals which are known to exhibit particularly slow convergence with respect to the integration grid [76, 77]), and the corresponding autogenerated MOLPRO grids were used. All calculations employed density fitting with the default auxiliary basis sets [78] in MOLPRO 2012. The -D2, -D3, -D3(BJ), -D3-$E^{(3)}$, and -D3(BJ)-$E^{(3)}$ corrections were computed using Grimme's DFTD3 program V3 Rev. 2. The LC-ωPBE and B2PLYP interaction energies were calculated by the PSI4 code [79], employing density fitting with the default PSI4 auxiliary basis sets. For the PSI4 calculations, the default 10^{-6} hartree energy convergence threshold and the Lebedev-Treutler (75,302) grid were utilized. As the CP correction is by no means guaranteed to improve DFT results, all DFT variants were tested both with and without this correction.

III. RESULTS AND DISCUSSION

A. Benchmark Interaction Energies

In this section we present how the benchmark wave-function-based N-PHAC–CO_2 interaction energies were obtained employing large-basis MP2 and CCSD(T) calculations. In order to understand the effects of basis set size on the MP2 interaction energy and on the ΔCCSD(T) contribution, we first examined the seven 1- and 2-ring systems that have at least C_s symmetry and obtained an extended set of conventional and explicitly correlated MP2 and CCSD(T) interaction energies including results in basis sets up to a5Z and aTZ, respectively. For the minimum geometry of the in-plane and stacked pyrazine-CO_2 systems, which are both small and highly symmetric, we computed the CCSD(T) results in an even larger, aQZ basis. The results for four representative systems are presented in Table I. This table includes the estimates of the total interaction energy obtained by a straightforward CBS extrapolation of the CCSD(T) results or an augmentation of the MP2/CBS value with the ΔCCSD(T) correction that is either computed or CBS-extrapolated. Table I illustrates the accuracy to which the CBS limit can be determined when the system size limits the CCSD(T) basis set choice to aTZ (as in the general case of the 1- and 2-ring systems) or aDZ (for all N-PHACs larger than 2-ring, except for the planar phenanthroline-CO_2 where we ran aTZ since it has C_{2v} symmetry). We examined the CCSD(T)-F12 approach with and without the scaling of triples, and noted that the scaling is harmful for the CCSD(T)-F12a variant but beneficial for CCSD(T)-F12b (the first observation indicates that the CCSD(T)-F12a approach, formally more approximate than CCSD(T)-F12b [60], highly benefits from a cancellation of errors between the CCSD part and the triples part [59]). Therefore, we use the average of the ΔCCSD(T)-F12a and ΔCCSD(T**)-F12b results, further denoted as ΔCCSD(T)-F12avg, as the benchmark value for the ΔCCSD(T) contribution. These values are listed in Table I along with the values of the ΔCCSD(T)-F12 and ΔCCSD(T**)-F12 interaction energy terms.

The nonextrapolated MP2 and MP2-F12 results in Table I all converge smoothly to the CBS limit. The (T,Q) and (Q,5) extrapolated values agree to within 0.04 kcal/mol for each system. Furthermore, the non-extrapolated MP2-F12 results are better than non-extrapolated MP2; however, after extrapolation both methods produce similar results.

The ΔCCSD(T) corrections shown in Table I exhibit a moderately fast convergence with the basis set size. It is obvious that extrapolation does help in the convergence of ΔCCSD(T). The explicitly correlated coupled cluster methods, especially CCSD(T)-F12a, exhibit faster convergence than traditional CCSD(T). The convergence of ΔCCSD(T)-F12a and ΔCCSD(T**)-F12b is smooth and the extrapolations work well. For the stacked pyrazine–CO_2 complex, the results gathered in Table I provide benchmark values of $-1.717\pm$ 0.006 kcal/mol for MP2 and 0.537 ± 0.003 kcal/mol for ΔCCSD(T). This leads to the total MP2/CBS+ΔCCSD(T) interaction energy of -1.180 ± 0.007 kcal/mol, where the uncertainties of the two contributions have been added quadratically.

It is not feasible to run CCSD(T)/aQZ for systems that contain more than one ring. It is also preferable to avoid doing CCSD(T)/aTZ for systems that contain more than two rings since these calculations are very demanding. If the CCSD(T)/aTZ calculations are feasible, as in the case of the seven symmetric 1- and 2-ring systems as well as the in-plane C_{2v} phenanthroline-CO_2 dimer, there are four sensible approaches to estimate the benchmark CCSD(T)/CBS limit from either conventional or explicitly correlated calculations: CCSD(T)/(D,T), MP2/(Q,5) + ΔCCSD(T)/(D,T), MP2/(Q,5) + ΔCCSD(T)/aTZ, and MP2/(Q,5) + ΔCCSD(T)/aDZ (note that the nonextrapolated CCSD(T)/aTZ values are inferior to the extrapolated and/or composite results, cf. Table I). For the in-plane and stacked pyrazine-CO_2 complexes, these combinations lead to absolute errors in the range 0.003–0.070 kcal/mol compared to the total interaction energy given by MP2-F12/(Q,5) + ΔCCSD(T)-F12avg/(T,Q). It is noted that the explicitly correlated CCSD(T)-F12 approach clearly improves the basis set convergence, and the CCSD(T)-F12a and CCSD(T**)-F12b values become virtually identical upon extrapolation. Because of this, we will use the average of ΔCCSD(T)-F12a and ΔCCSD(T**)-F12b as the final ΔCCSD(T) contribution to the benchmark: that is, the benchmark interaction energy for the 1- and 2-ring systems will be MP2-F12/(Q,5)+ΔCCSD(T)-F12avg/(D,T). Since the CCSD(T)/aQZ calculations are very time-consuming, we will use the theory level defined above to produce the benchmark potential energy curve also for pyrazine-CO_2. For this system, the errors resulting from the restriction of coupled-cluster calculations to the aTZ basis set are 0.003–0.010 and 0.008–0.014 kcal/mol for MP2-F12/(Q,5)+ΔCCSD(T)-F12avg/(D,T) and MP2/(Q,5)+ΔCCSD(T)/(D,T), respectively. A further restriction to aDZ leads to errors of 0.028–0.058 and 0.048–0.063 kcal/mol for explicitly correlated and conventional CCSD(T),

respectively. Even this last error, corresponding to less than 6% of the total interaction energy, is remarkably low.

The quinoxaline–CO_2 results in Table I exhibit similar convergence patterns. The conventional ΔCCSD(T) part shows smooth convergence and the aDZ and aTZ bases are sufficient to narrow this term down to about 0.02 kcal/mol. The highest-level conventional estimates of the CBS limit, the MP2/(Q,5) + ΔCCSD(T)/(D,T) results, are too low by 0.018–0.026 kcal/mol compared to the benchmark MP2-F12/(Q,5)+ΔCCSD(T)-F12avg/(D,T) value. The observed accuracy of the conventional MP2/(Q,5)+ΔCCSD(T)/(D,T) estimate is similar to that found for the pyrazine-CO_2 dimer. The same trend is also true for the MP2-F12/(Q,5)+ΔCCSD(T)-F12avg/aDZ (errors of 0.02–0.05 kcal/mol) and MP2/(Q,5)+ΔCCSD(T)/aDZ (errors of 0.03–0.08 kcal/mol) estimates. Consequently, the satisfactory, better than 0.1 kcal/mol accuracy of even the simplest approach, MP2/(Q,5) +ΔCCSD(T)/aDZ, is likely transferable to dimers that involve larger N-PHACs. Therefore, all benchmarks for systems larger than two rings, and for the nonsymmetric stacked quinoline-CO_2 complex, will utilize the conventional MP2/(Q,5)+ΔCCSD(T)/aDZ level except for the C_{2v} phenanthroline-CO_2 system and the largest dimers, which will employ MP2/(Q,5)+ ΔCCSD(T)-F12avg/(D,T) and MP2/(Q,5)+ΔCCSD(T)/laDZ, respectively—see below. As seen from Table I, the F12 approach does greatly improve the calculated MP2 results. The conventional MP2 results are nearly as accurate as long as the CBS extrapolation is performed, but the uncertainties of conventional MP2 (computed as differences between the extrapolated MP2/(Q,5) energy and the calculated MP2/a5Z energy) are larger than those of the MP2-F12 interaction energies. In the case of quinoxaline-CO_2, the MP2 and MP2-F12 uncertainties amount to 0.054 and 0.001 kcal/mol for the in-plane dimer and 0.064 and 0.013 kcal/mol for the stacked dimer, respectively. Nevertheless, all MP2 interaction energies for three-ring and larger systems, and for the stacked quinoline-CO_2 structure, will be obtained from a conventional extrapolation at the (Q,5) level as the cost of MP2-F12/a5Z starts to become prohibitive.

Figure 2 displays the differences between the benchmark MP2-F12/(Q,5)+ΔCCSD(T)-F12avg/(D,T) result and various other CCSD(T)/CBS estimates for in-plane pyridine-CO_2 (left panel) and stacked quinoxaline-CO_2 (right panel) as functions of η (η is defined throughout the text as $\frac{z}{z_{min}}$, where z_{min} represents the minimum-energy z distance for each dimer). At the minimum separations for both complexes, all extrapolations shown agree with the

benchmark to within 0.1 kcal/mol. For larger η, all considered variants are nearly as accurate as the benchmark MP2-F12/(Q,5)+ΔCCSD(T)-F12avg/(D,T) value. It is the short range, $\eta < 1.0$, where different benchmark variants start deviating more from each other. If only the aDZ basis set is available for the ΔCCSD(T) contribution, MP2/(Q,5)+ΔCCSD(T)/aDZ is superior to MP2-F12/(Q,5)+ΔCCSD(T)-F12avg/aDZ for in-plane pyridine-CO_2 but inferior for stacked quinoxaline-CO_2.

Since the performance of various CCSD(T)/CBS estimates for the in-plane and stacked dimers is quite different, we examine the mean unsigned errors (MUE) of different CCSD(T)/CBS schemes for all the symmetric 1- and 2-ring systems (7 dimers altogether) compared to the benchmark MP2-F12/(Q,5)+ΔCCSD(T)-F12avg/(D,T) results in Fig. 3. At the minimum distance, $\eta = 1.0$, the values for all different schemes agree to within 0.06 kcal/mol. However, different CCSD(T)/CBS estimates start deviating from each other in the repulsive region. From a statistical point of view, the MP2-F12/(Q,5)+ΔCCSD(T)-F12avg/aDZ results are slightly superior to the MP2/(Q,5)+ΔCCSD(T)/aDZ ones, but the differences are small and consistent across the whole distance range. Thus, the limited increase in the short-range accuracy does not warrant the additional computational effort of a CCSD(T)-F12 calculation and the benchmark interaction energies for larger systems will include the ΔCCSD(T) contribution from conventional CCSD(T).

The CCSD(T)/aDZ interaction energies cannot be computed for the 1,6-diazacoronene–CO_2 system due to the presence of diffuse basis functions on multiple centers leading to near linear dependencies in the basis set. In order to overcome the linear dependency issue, at least some of the offending diffuse basis functions have to be removed. However, the most popular scheme of removing diffuse functions from aXZ, the "calendar" basis sets [80], may lead to persisting linear dependencies, a significant drop in accuracy, or both, as shown for the methane–pyrene and methane–coronene complexes [39]. Instead, an alternative basis set truncation scheme is employed where only the carbon dioxide atoms and the six closest heavy atoms (relative to the carbon in carbon dioxide) of the N-PHAC molecule retain diffuse functions; this approach is labeled as local-aug-cc-pVDZ (laDZ) [39, 40]. Pictorial demonstrations of the augmentation schemes in the 2-azapyrene–CO_2 and 1,6-diazacoronene–CO_2 complexes are displayed in Fig. 1. The bronze-colored carbon atoms in the N-PHAC molecule as well as the closest nitrogen atom (blue) are those that have diffuse functions in the laDZ basis. A comparison of the MP2 interaction energies and ΔCCSD(T)

corrections calculated using the full aDZ basis, its laDZ subset, and the nonaugmented cc-pVDZ set across the whole range of η is shown in Table II. This table gathers the results for 2-azapyrene–CO_2, for which we can get the CCSD(T) results for both aDZ and laDZ, and 1,6-diazacoronene–CO_2, for which we can only obtain the ΔCCSD(T) values in the laDZ basis.

The 2-azapyrene–CO_2 results in Table II demonstrate that diffuse functions are significant for both the MP2 interaction energy and the ΔCCSD(T) correction. The energy differences between full aDZ and cc-pVDZ are up to 4.8 kcal/mol for the MP2 interaction energy and up to 0.6 kcal/mol for the ΔCCSD(T) contribution. At the minimum distances, the deviations between ΔCCSD(T)/cc-pVDZ and ΔCCSD(T)/aDZ are 0.01 and 0.28 kcal/mol for the in-plane and stacked 2-azapyrene–CO_2 complexes, respectively. These values should be contrasted with the corresponding differences between ΔCCSD(T)/laDZ and ΔCCSD(T)/aDZ, amounting to 0.01 kcal/mol in both cases. Thus, while for the in-plane structure the ΔCCSD(T) correction is quite unimportant, for the stacked geometry the partial augmentation present in the laDZ set is both necessary and sufficient to obtain an accurate value of this term. For the two dimers presented, the differences between the ΔCCSD(T) terms in two basis sets are roughly an order of magnitude smaller than the differences in the MP2 interaction energy. Thus, the results in Table II suggest that the ΔCCSD(T)/laDZ values for 1,6-diazacoronene-CO_2 should be within about 0.02 kcal/mol from the full aDZ results. Consequently, the benchmark 1,6-diazacoronene–CO_2 interaction energies will be obtained at the MP2/(Q,5)+ΔCCSD(T)/laDZ level.

The results in Tables I–II show that the ΔCCSD(T) correction is quite small, typically less than 0.1 kcal/mol at the minimum distance, for the in-plane dimers. For the stacked configurations, the ΔCCSD(T) correction is significantly larger and MP2 overbinds by up to 1.8 kcal/mol at the minimum distance. This is the case across all the in-plane and stacked structures (eight planar and eight stacked configurations, as shown in Fig. 1). In order to investigate this phenomenon for all systems, the mean unsigned relative errors (MURE) of MP2 and spin component scaled MP2 (SCS-MP2) [81] compared to the benchmark values are displayed in Fig. S1 in the Supporting Information. As explained in more detail below, the averaging includes 95 geometries (the η=0.9 point of stacked pyridine–CO_2 is discarded because it is accidentally very close to zero). As the ΔCCSD(T) correction is small for in-plane complexes, the MP2/(aQZ, a5Z) result is very good with an overall MURE of 4.4%

while the SCS-MP2/(aQZ, a5Z) results are quite poor (a MURE of 23.8%). The opposite is true for stacked complexes, with a MURE of 12.7% for SCS-MP2/(aQZ, a5Z) and 44.6% for MP2/(aQZ, a5Z). The MURE of the CP-uncorrected MP2 and SCS-MP2 interaction energies is also shown in Fig. S1. One can conclude from this figure that the lack of a CP correction significantly worsens the accuracy of MP2 but provides some limited improvement at the SCS-MP2 level.

The benchmark interaction energies computed so far do not include any monomer flexibility effects. These effects can be examined by comparing the van der Waals well depth obtained with the monomers frozen at their own optimized geometries (as is the case throughout the rest of this work) to the well depth calculated by a minimization of the CP-corrected interaction energy between fully flexible monomers. In the latter case, the quantity that needs to be minimized is

$$\begin{aligned} E_{\rm int}^{\rm flexible} = [E^{\rm AB}(AB) - E^{\rm AB}(A) - E^{\rm AB}(B)] \\ +[E^{\rm A}(A) - E_0^{\rm A}(A)] + [E^{\rm B}(B) - E_0^{\rm B}(B)] \end{aligned} \tag{3}$$

where the subscript 0 represents the nonrelaxed minimum geometry of the monomer, the superscripts signify the basis set (dimer-centered or monomer-centered), and the symbols in parentheses denote the subsystems. On the example of the in-plane pyridine-CO_2 dimer, we first examined the effects of the CO_2 flexibility, with the pyridine monomer remaining rigid. The resulting flexible well depth, obtained by minimizing Eq. (3) with the system constrained to the C_{2v} symmetry, is larger by 0.166 kcal/mol (at the MP2/aTZ level) than the conventional rigid well depth. Furthermore, the changes in the C-O bond lengths do not exceed 0.0003 Å and the O-C-O angle change is 3.15°. The flexible-CO_2 energy is further lowered by 0.031 kcal/mol in a completely unrestricted MP2/aTZ dimer optimization. Thus, the total flexibility contribution to interaction energy is 0.197 kcal/mol, which is in good agreement with the previous theoretical result of 0.20 kcal/mol obtained for this system at the MP2/cc-pVTZ level [42]. The C-O bond length and the O-C-O angle keep almost the same values in the CO_2-only and fully flexible optimizations. Therefore, the flexibility effect comes mainly from the relaxation of the CO_2 molecule and the flexibility of the N-PHAC monomer will be neglected.

In the case of the stacked pyridine-CO_2 complex, we first optimized the tilt angle of CO_2, resulting in an interaction energy (still rigid and symmetric but not restricted to parallel configurations anymore) lower by 0.002 kcal/mol. Then, based on the geometry of this

tilted configuration, the CO_2-only flexible minimization was performed and the relaxation energy was 0.011 kcal/mol. Finally, a totally unrestricted MP2/aTZ dimer optimization of the stacked pyridine-CO_2 dimer was performed, lowering the interaction energy by a further 0.023 kcal/mol. Thus, the total flexibility contribution to interaction energy for the stacked pyridine-CO_2 dimer is 0.034 kcal/mol. The CO_2-only relaxation energies for the N-PHAC-CO_2 dimers are gathered in Table III to demonstrate the flexibility effects. The flexibility effects for stacked complexes turn out to be very small except for the phenanthroline–CO_2 system.

We conclude that while the flexibility effects are significant for the in-plane orientations, they are negligible for the stacked ones. One may note that the stacked configurations are more representative of extended nanotubes than the in-plane ones, and that the precise details of the geometry (flexible or rigid) are not relevant for the main purpose of this work, an assessment of the performance of different DFT-based approaches. Moreover, as we proceed to examine radial cross sections through the intermolecular potential energy surfaces, it would be cumbersome to reoptimize the monomer geometry at each intermolecular separation. Therefore, all calculations throughout the rest of this work utilize rigid monomers.

The accuracy of the benchmark energies obtained in this section does not only rely on the accuracy with which the CCSD(T)/CBS limit is estimated, but also on the smallness of the effects neglected in the frozen-core CCSD(T) calculation. In order to examine the effect of core-core and core-valence correlation on the interaction energy, we computed the all-electron CCSD(T)/aug-cc-pCVDZ and CCSD(T)/aug-cc-pCVTZ interaction energies for the four 1-ring systems at $\eta = 1.0$. In the aug-cc-pCVDZ basis, the all-electron and frozen-core interaction energies differ by 0.004–0.005 kcal/mol; for the aug-cc-pCVTZ set the corresponding differences range from 0.002 to 0.011 kcal/mol. Thus, the interaction energy contributions from the core-core and core-valence correlation should not exceed a few hundredths of a kilocalorie per mole. The relativistic effects are likely even smaller as only light atoms are present. The effects of coupled-cluster excitations beyond CCSD(T) are the hardest to estimate, especially since their basis set convergence is often slow [82, 83]. The most similar system for which these effects have been estimated is the benzene dimer, for which Pitoňák *et al.* [84] performed small-basis CCSD(TQ_f) [85] calculations, taking into account approximate quadruple excitations. The post-CCSD(T) interaction energy corrections obtained in this way ranged from 0.02 to 0.04 kcal/mol so we expect the post-CCSD(T)

effects to be of similar magnitude for the systems considered here. Overall, our benchmark interaction energies are likely accurate to 0.1 kcal/mol or better at the minimum separations ($\eta = 1.0$).

B. DFT calculations

In this section, we examine how well different DFT functionals recover the MP2/CBS+ΔCCSD(T) benchmark interaction energies for the N-PHAC-CO_2 complexes. The 16 minima obtained in Sec. III A were investigated at η times the minimum distance z_{min}, η = 0.8, 0.9, 1.0, 1.2, 1.4, and 1.6, giving a total of 96 CCSD(T) results. The DFT interaction energies were computed using the def2-SVP, TZVP, QZVP [86] and Dunning aDZ and aTZ basis sets combined with five possible variants of Grimme's dispersion correction: -D2 [27], -D3 [33], -D3(BJ) [74], -D3-E$^{(3)}$, and -D3(BJ)-E$^{(3)}$, both with and without the CP correction. As the M0x series are interaction-optimized functionals, we also examined their performance without an additional atom-pairwise dispersion term. This corresponds to a total of 450 different combinations of functionals, basis sets, dispersion corrections, and the CP correction or lack thereof (note that the dispersion corrections for the M0x series include only -D3 and -D3-E$^{(3)}$, and there is no -D2 correction for LC-ωPBE).

The accuracy of different DFT variants with respect to the CCSD(T)-level benchmark interaction energy, obtained as described above, will be investigated using mean unsigned relative error (MURE). The results include all 96 points except for a point in the repulsive region (the η=0.9 geometry of stacked pyridine–CO_2) which is very close to zero and would accidentally dominate the MURE. The MURE values of all 450 different combinations of functionals, basis sets, dispersion corrections, and the CP correction or lack of it (nonCP) are collected in the Supporting Information. Overall, the MUE/MURE values in the QZVP basis range from 0.17 kcal/mol / 6.4% for nonCP B2PLYP-D3 to 1.25 kcal/mol / 45.9% for CP B97-D2. This range of errors is very similar for smaller basis sets down to aDZ, but a further basis reduction to SVP increases the errors to the range between 0.28 kcal/mol (CP M06-2X-D3)/11.1% (CP LC-ωPBE-D3-E$^{(3)}$) and 1.33 kcal/mol (CP B97-D2)/52.2 % (nonCP BLYP-D3(BJ)). To examine which DFT variants provide the most consistent accuracy, we analyzed the MURE values for each η and each geometry type (in-plane/stacked) separately — the pertinent results are given in the Supporting Information. The deterioration of

accuracy at the short range is clear for most of the methods: at the shortest separation $0.8z_{min}$ in the QZVP basis, only the different variants of M05-2X, M06-2X, PBE0 (both CP and nonCP), LC-ωPBE, and B2PLYP-D3 (nonCP only) attain a MURE below 20%. As expected, the M05-2X and M06-2X approaches without additional dispersion perform poorly in the long range (MURE in the QZVP basis is over 20% for all $\eta \geq 1.2$). However, the M05-2X-D3 and M06-2X-D3 variants perform fairly well at all separations. The MURE values as functions of η for these functionals, along with the next best approaches B3LYP-D3(BJ), LC-ωPBE-D3 (with and without the CP correction), and B2PLYP-D3 (nonCP only) are presented in Fig. 4. Additionally, this figure shows the corresponding MURE separated into in-plane and stacked complexes. The PBE0-D3 functional was omitted from Fig. 4 as its reasonable (MURE 16–23% depending on the -D3 variant and CP/nonCP) accuracy at $\eta = 0.8$, mentioned above, deteriorates to 35–43% at $\eta = 0.9$.

The results in Fig. 4 indicate that the performance at different η varies significantly: in particular, the relative accuracy of virtually all DFT-based methods decreases at distances somewhat shorter than the minimum. Both the -D3 extensions of standard DFT variants such as B3LYP and PBE and the double hybrid functional B2PLYP-D3 perform very well at the van der Waals minima and at larger distances, with most MURE values below 5%. However, the errors increase several times in the mildly repulsive region of the interaction, with B2PLYP-D3 performing somewhat better than lower-rung functionals but still unsatisfactorily. The M06-2X-D3 approach presents a particularly interesting case: it provides, along with M05-2X-D3, by far the best accuracy at $\eta = 0.8$ but the errors vary irregularly with the separation, with large MURE values at $\eta = 1.2$ and 1.6 (but not 1.4). The behavior of M05-2X-D3 is much more stable although the errors at $\eta = 0.9$ are somewhat large. While Fig. 4 indicates that M05-2X-D3, along with B2PLYP-D3, should be the method of choice for studying N-PHAC–CO_2 potential energy surfaces, the oscillating accuracy of M06-2X-D3 shows, in our opinion, the dangers of strongly parameterized functionals [87]. Figure 4 also shows that all top-performing DFT variants except for B2PLYP-D3 provide somewhat better relative accuracy for the in-plane geometries than for the stacked ones, but the orderings of functionals according to their MURE for in-plane and stacked complexes are remarkably similar.

The deterioration of the DFT+D accuracy in the mildly repulsive region of the interaction presents a serious problem as this region is extensively sampled in dynamics calculations

and relevant for the computation of many interaction-dependent observables such as second virial coefficients and scattering cross sections. As argued in our recent work on interactions between CO_2 and pristine carbon nanotubes [41], there are likely two reasons for this deterioration: overestimation of exchange by standard GGA functionals [88, 89] and inadequacy of the damping functions used in the -D3 dispersion correction. The first of these issues can be alleviated by improving on the asymptotic behavior of the exchange functional by increasing the fraction of exact exchange at long range. This can be accomplished through the range separation (long-range correction) technique [90–92] as exemplified by the LC-ωPBE functional [73] (for which the -D3 parameters are available). This is the reason why we included the LC-ωPBE functional in the set of methods tested. However, Fig. 4 shows that the performance of LC-ωPBE at $\eta = 0.8$ and 0.9 is still not satisfactory. Therefore, we believe that at least a part of the problem lies in the damping forms of -D3 which have been optimized mostly for data at the van der Waals minimum separations [33, 74]. Consequently, in Ref. 41 two of us have proposed a refitting of the -D3, -D3(BJ), and Tang-Toennies [93] damped dispersion -D3(TT) to optimally reproduce the curved coronene–CO_2 benchmark interaction energies, also at intermolecular separations as short as 0.8 times the minimum. Therefore, *without any additional refitting,* we checked how the damping parameters of Ref. 41 perform relative to the original parameters from Refs. 33 and 74 on our N-PHAC–CO_2 benchmark dataset. The results are shown in Fig. 5, in the largest basis set QZVP with the CP correction. With the refitting, PBE-D3$_{\rm refit}$/CP is the top DFT performer (5.1%), followed by the B2PLYP-D3(TT)$_{\rm refit}$/CP (5.8%). Refitting improves results for almost all the variants except for the -D3(BJ)$_{\rm refit}$ approach for some functionals. While it was shown in Ref. 41 that -D3$_{\rm refit}$ (though not -D3(BJ)$_{\rm refit}$ or -D3(TT)$_{\rm refit}$) performs as well as original -D3 for the popular S22x5 [94] and S66x8 [36] databases, the transferability of the refitted damping parameters should not be taken for granted. Therefore, it is highly gratifying that the parameters from Ref. 41 improve the performance of standard DFT-D3 also for the N-PHAC–CO_2 complexes without any refitting required.

Figure 6 illustrates the basis set dependence of the accuracy of the top-performing functionals. This figure indicates that larger basis sets improve the DFT+D performance, with the MURE generally decreasing in the order SVP $\rightarrow$ aDZ $\rightarrow$ TZVP $\rightarrow$ aTZ $\rightarrow$ QZVP. In the largest basis set, QZVP, the MURE values for CP and nonCP are almost identical to each other, except that B2PLYP/nonCP is superior to B2PLYP/CP. One should note that

conventional functionals such as B3LYP and M05-2X exhibit faster basis set convergence than the B2PLYP double hybrid method, and their accuracy does not decay so dramatically in smaller basis sets (even SVP) as long as the CP correction is applied. This result is in agreement with the findings of Refs. 38 and 41 who found that the CP-corrected DFT results converge smoothly and different bases require similar damping parameters in the accompanying -D3 term.

The mean unsigned relative error for the best DFT functionals as a function of the N-PHAC size (the number of rings) is displayed in Fig. S2 in the Supporting Information. In particular, we are interested to find out if there is any deterioration of the DFT-D3 accuracy with increasing system size due to the neglect of pairwise-nonadditive effects [95] and, if so, if the three-body -$E^{(3)}$ dispersion correction [33] helps alleviate this deterioration as suggested in a recent benchmark study of large weakly interacting complexes [37]. However, the results in Fig. S2 show that the relative accuracy of top-performing DFT variants is highly uniform across systems of different sizes with an exception of M05-2X-D3 which strangely displays poor performance for the four-ring (2-azapyrene–CO_2) complexes. Moreover, the influence of the -$E^{(3)}$ term is minor in all cases. We conclude that the pairwise-nonadditive dispersion effects are relatively unimportant for the N-PHAC–CO_2 complexes considered in this work.

To conclude the DFT analysis, the interaction energies at the MP2/CBS level, the MP2/CBS+ΔCCSD(T) benchmarks, and the top DFT performers: B2PLYP-D3/$^{\mathrm{nonCP}}_{\mathrm{QZVP}}$, B3LYP-D3(BJ)/$^{\mathrm{nonCP}}_{\mathrm{QZVP}}$, and M05-2X-D3/$^{\mathrm{CP}}_{\mathrm{QZVP}}$ for each N-PHAC are shown in Fig. S3 in the Supporting Information. As mentioned above, the size of the ΔCCSD(T) correction is very small for in-plane geometries. As a result, the MP2 and CCSD(T) results for the eight in-plane configurations differ by only up to 0.07 kcal/mol. Conversely, the stacked dimers strongly benefit from the ΔCCSD(T) contribution: as expected, the MP2 values overestimate the interaction energies. For all of the investigated systems, the global minimum configurations are in-plane, even though MP2/CBS predicts an incorrect minimum structure for the 2-azapyrene and 1,6-diazacoronene complexes. For both in-plane and stacked structures, the best DFT performers do an excellent job of reproducing the CCSD(T)-level benchmark interaction energy. Overall, the best performing DFT/QZVP functional at the minimum separations ($\eta = 1.0$), B3LYP-D3(BJ)-$E^{(3)}$/nonCP, reproduces the minimum benchmark values to within 0.06 kcal/mol or 1.7% on the average. This level of accuracy is clearly fortuitous and does not carry on to other distances, but it illustrates that modern

DFT variants are very capable of providing accurate van der Waals minimum energies as opposed to interaction energies in the mildly repulsive region.

C. Performance of Selected DFT Variants on Model N-Doped Graphene Holes

The DFT approaches that best reproduce the CCSD(T)-level benchmark results for CO_2 interacting with N-PHACs should be the methods of choice for studying interactions involving larger N-PHACs as well as with extended structures such as nitrogen-doped graphene sheets and carbon nanotubes. We performed the first step in this direction and computed, for the best DFT performers identified in Sec. III B, the CO_2 interaction energies with three larger N-PHACs representing the barriers to the CO_2 transition through model vacancies in the N-doped graphene surface. The geometries for these N3, N4, and N4H4 vacancy models interacting with CO_2 are presented in Fig. 7. The geometry of the vacancy was optimized at the MP2/aDZ, B3LYP/aTZ, and B3LYP/aDZ level for N3, N4, and N4H4, respectively, and the CO_2 molecule was confined to the perpendicular orientation along the symmetry axis of the vacancy. Figure 8 displays the interaction energies for the best DFT performers determined in Sec. III B: B3LYP-D3(BJ)/$^{\rm nonCP}_{\rm aTZ}$, M05-2X-D3/$^{\rm CP}_{\rm aTZ}$, and B2PLYP-D3/$^{\rm nonCP}_{\rm aTZ}$ as well as the CP-corrected MP2/aTZ interaction energies. From this figure, the energy barrier for CO_2 traveling through the (rigid) N3 vacancy is 507, 472, 485, and 450 kcal/mol for M05-2X-D3/$^{\rm CP}_{\rm aTZ}$, B2PLYP-D3/$^{\rm nonCP}_{\rm aTZ}$, B3LYP-D3(BJ)/$^{\rm nonCP}_{\rm aTZ}$, and MP2/aTZ, respectively. The highest energy barrier occurs when one of the oxygen atoms in carbon dioxide passes through the N3 plane. For the N4 vacancy-CO_2 complex, the respective energy barriers are 216, 209, 213, and 202 kcal/mol. Thus, the rigid N3 and N4 holes are impassable to CO_2, but we still need to consider the stretching of the vacancy by the passing CO_2 molecule that may significantly lower the barrier.

In the case of the N3 vacancy-CO_2 dimer, we will first examine the flexibility effects with the CO_2 carbon remaining in the center of the vacancy and allowing both the N-PHAC and the C–O bonds to stretch. The resulting flexible $z = 0$ barrier, obtained by minimizing Eq. (3) with the system constrained to the C_{2v} symmetry, is smaller by 97.7 kcal/mol (at the B3LYP/aDZ level) than the conventional rigid $z = 0$ barrier. Furthermore, the C–O bond length is larger by 0.237 Å and the distance from the center of the N3 vacancy to the nitrogen atoms is elongated by 0.148 Å. Based on the geometrical parameters from the

B3LYP/aDZ flexible optimization, the single point calculations using MP2/aDZ, B3LYP-D3/aTZ, and M05-2X-D3/aTZ (all CP-corrected) were performed. The resulting interaction energies including the monomer deformation effects are 177.4, 174.0, and 186.4 kcal/mol, respectively.

When it comes to the N4 vacancy-CO_2 dimer, the flexibility effects, estimated by minimizing Eq. (3) with the system constrained to the C_{2v} symmetry, lower the rigid $z = 0$ barrier by 25.3 kcal/mol at the B3LYP/aDZ level. At the same time, the C–O bond length increases by 0.026 Å and the distance from the center of the N4 vacancy to the nitrogen atoms grows by 0.182 Å. Using the flexible geometry of the complex, we again performed single-point calculations at the B3LYP-D3/aTZ and M05-2X-D3/aTZ levels including the counterpoise and monomer deformation corrections, obtaining interaction energy values of 94.5 and 98.8 kcal/mol, respectively. Thus, the flexible energy barrier is still large enough to prevent the CO_2 molecule from passing through the N4 hole.

At $z = 4.0$ Å, close to the van der Waals minimum in Fig. 8, when CO_2 is oriented perpendicular to the N3 vacancy, the B2PLYP-D3/$^{\mathrm{nonCP}}_{\mathrm{aTZ}}$ interaction energy is -1.84 kcal/mol. However, an orientation of CO_2 parallel to the surface, at the same distance, is more favorable with an interaction energy of -2.99 kcal/mol. At the same $z = 4.0$ Å, the B2PLYP-D3/$^{\mathrm{nonCP}}_{\mathrm{aTZ}}$ energies are -1.54 and -3.10 kcal/mol for the perpendicular and parallel N4 vacancy-CO_2 complexes, respectively.

It is interesting to explore a larger vacancy that allows the CO_2 molecule to move from one side of the N-PHAC to the other much easier than in the N3 and N4 cases. According to Ref. 14, the CO_2 molecule could pass the N4H4 vacancy almost freely. Therefore, we picked the N4H4 vacancy model, Fig. 7, as a representative of a larger hole to study the N-PHAC–CO_2 interaction energy. We kept the monomers rigid and restricted the symmetry to D_{2h}. Figure 9 displays the interaction energies for the best DFT performers determined in Sec. III B: B3LYP-D3(BJ)/$^{\mathrm{nonCP}}_{\mathrm{aTZ}}$, M05-2X-D3/$^{\mathrm{CP}}_{\mathrm{aTZ}}$, and B2PLYP-D3/$^{\mathrm{nonCP}}_{\mathrm{aTZ}}$ as well as the CP-corrected MP2/aTZ interaction energies. From this figure, all methods predict a minimum when CO_2 is located at the center of the vacancy (in good agreement with the results of Ref. 14) with an interaction energy around -7.5 kcal/mol.

For comparison to the N3 and N4 vacancy models, we computed the B2PLYP-D3/$^{\mathrm{nonCP}}_{\mathrm{aTZ}}$ energies for the two parallel C_{2v} N4H4-hole-CO_2 complexes as well, at $z = 4.0$ Å. The interaction energies are -1.14 kcal/mol for the perpendicular orientation and -1.52, -1.72

kcal/mol for the two parallel C_{2v} N4H4 vacancy-CO_2 complexes (the oxygen atoms orient towards the nitrogens for the first one and towards the intra-vacancy hydrogens for the second one, respectively). Thus, the parallel orientations are energetically favorable at this distance. Overall, while the N3 and N4 vacancies are clearly too small for CO_2 (or, likely, any molecule) to pass through, the N4H4 hole is large enough, and provides a large enough dispersion interaction, to afford an (energetically) barrierless transition of CO_2 to the other side. This observation coincides, and the resulting well depth agrees quantitatively, with the findings of Ref. 14 which used the PBE-D2 level of theory and a wide (19,0) porous nanotube in place of graphene. The agreement between different approaches illustrated in Fig. 9 could not have been taken for granted, but it is highly gratifying, confirming that the DFT-based variants selected on the basis of their reproduction of benchmark data for smaller N-PHAC-CO_2 complexes are also appropriate, and consistent, for the study of carbon dioxide permeation through realistic models of porous N-doped graphene.

IV. SUMMARY

High-accuracy benchmark interaction energies were obtained for weakly interacting complexes of CO_2 with nitrogen-containing polyheterocyclic aromatic compounds, N-PHACs (pyrazine, pyridine, quinoline, quinoxaline, pyrido[3,2-g]quinoline, phenanthroline, 2-azapyrene, and 1,6-diazacoronene). The energies were computed by the supermolecular MP2 approach extrapolated to the complete basis set limit plus a CCSD(T) correction calculated in a moderate basis set (up to aTZ for most 1- and 2-ring N-PHACs, aDZ for most 3- and 4-ring systems, and laDZ for 1,6-diazacoronene-CO_2). The calculations for 1- and 2-ring N-PHAC-CO_2 complexes (except for stacked quinoline-CO_2) utilized the explicitly correlated CCSD(T)-F12a/b approaches while all other systems were treated using conventional CCSD(T). An extensive basis set convergence analysis indicates that our benchmark interaction energies are accurate to a few hundredths of a kilocalorie per mole at the minimum separations. Our CCSD(T)-level results indicate that the global minimum structures for CO_2 interacting with N-PHACs are all in-plane. The ΔCCSD(T) correction is quite small (less than 0.08 kcal/mol at the minimum distance) for in-plane dimers. For the stacked configurations, the ΔCCSD(T) correction is significantly larger and the MP2 energies overbind by up to 1.8 kcal/mol at the minimum distance.

The newly developed CCSD(T)-level benchmarks were subsequently used to investigate the accuracy of several novel DFT approaches for the N-PHAC-CO_2 interaction energies. The comparisons included one-dimensional cuts through the N-PHAC-CO_2 potential energy surfaces passing through the lowest-energy structures for both the in-plane and stacked complexes, with distances ranging from 0.8 times the minimum to 1.6 times the minimum. Thus, the optimal DFT variant needs to provide a uniformly high accuracy for the entire potential energy curve, not just around the van der Waals minima. The tested approaches included M05-2X, M06-2X, B2PLYP, B3LYP, BLYP, PBE, PBE0, BP86, B97, and LC-ωPBE with the def2-SVP, TZVP, QZVP and Dunning aDZ and aTZ basis sets combined with five possible variants of Grimme's dispersion correction: -D2, -D3, -D3(BJ), -D3-$E^{(3)}$, and -D3(BJ)-$E^{(3)}$, both with and without the CP correction. In the largest, QZVP basis set, the three best approaches overall turned out to be B2PLYP-D3/nonCP, B2PLYP-D3(BJ)/nonCP, and M05-2X-D3/(both CP and nonCP), with mean unsigned relative errors on the 95 benchmark data points amounting to 6.4, 6.9, and 7.2%, respectively. Thus, a few DFT+D variants exhibit reasonable accuracy throughout the entire range of distances unlike the case of pristine carbon nanotubes interacting with CO_2 [41]. While a redesign of the atom-pairwise dispersion expression is not necessary for this work, the refitting of damping parameters performed for curved coronene-CO_2 complexes in Ref. 41 improved the performance of most DFT+D variants also for the N-PHAC-CO_2 models considered here.

The top performing DFT variants along with the MP2 approach were subsequently employed to study the barrier to a carbon dioxide transition through three model N-doped graphene pores. We found that only the largest of them, the N4H4 pore, is permeable to CO_2. For this pore, we obtained a quantitative agreement between all computed energy profiles and the results of Ref. 14. As the treatment of dispersion within the methods tested by us ranges from additive (DFT+D) to partially nonadditive (B2PLYP-D3) to fully nonadditive (MP2) and no systematic discrepancies were observed as the model size increased, the pairwise-nonadditive effects on dispersion [95–98] are apparently not critical for the complexes considered in this work.

ACKNOWLEDGMENT

This research was supported by the Donors of the American Chemical Society Petroleum Research Fund, the NSF CAREER award CHE-1351978, and the startup funding from Auburn University.

[1] Czerw, R.; Terrones, M.; Charlier, J.-C.; Blase, X.; Foley, B.; Kamalakaran, R.; Grobert, N.; Terrones, H.; Tekleab, D.; Ajayan, P. M.; Blau, W.; Rühle, M.; Carroll, D. L. *Nano Lett.* **2001**, *1*, 457–460.

[2] Kang, H. S.; Jeong, S. *Phys. Rev. B* **2004**, *70*, 233411.

[3] Sun, C.; Wang, H.; Hayashi, M.; Chen, L.; Chen, K. *J. Am. Chem. Soc.* **2006**, *128*, 8368–8369.

[4] Usachov, D.; Vilkov, O.; Grüneis, A.; Haberer, D.; Fedorov, A.; Adamchuk, V. K.; Preobrajenski, A. B.; Dudin, P.; Barinov, A.; Oehzelt, M.; Laubschat, C.; Vyalikh, D. V. *Nano Lett.* **2011**, *11*, 5401–5407.

[5] Cho, Y. J.; Kim, H. S.; Baik, S. Y.; Myung, Y.; Jung, C. S.; Kim, C. H.; Park, J.; Kang, H. S. *J. Phys. Chem. C* **2011**, *115*, 3737–3744.

[6] Luo, Z.; Lim, S.; Tian, Z.; Shang, J.; Lai, L.; MacDonald, B.; Fu, C.; Shen, Z.; Yu, T.; Lin, J. *J. Mater. Chem.* **2011**, *21*, 8038–8044.

[7] Robertson, J.; Davis, C. A. *Diamond Relat. Mater.* **1995**, *4*, 441–444.

[8] Jiang, D.; Cooper, V. R.; Dai, S. *Nano Lett.* **2009**, *9*, 4019–4024.

[9] Blankenburg, S.; Bieri, M.; Fasel, R.; Müllen, K.; Pignedoli, C. A.; Passerone, D. *Small* **2010**, *6*, 2266–2271.

[10] Du, H.; Li, J.; Zhang, J.; Su, G.; Li, X.; Zhao, Y. *J. Phys. Chem. C* **2011**, *115*, 23261–23266.

[11] Schrier, J. *ACS Appl. Mater. Interfaces* **2011**, *3*, 4451–4458.

[12] Schrier, J. *ACS Appl. Mater. Interfaces* **2012**, *4*, 3745–3752.

[13] Liu, H.; Cooper, V. R.; Dai, S.; Jiang, D. *J. Phys. Chem. Lett.* **2012**, *3*, 3343–3347.

[14] Bucior, B. J.; Chen, D.-L.; Liu, J.; Johnson, J. K. *J. Phys. Chem. C* **2012**, *116*, 25904–25910.

[15] Hauser, A. W.; Schwerdtfeger, P. *Phys. Chem. Chem. Phys.* **2012**, *14*, 13292–13298.

[16] Hauser, A. W.; Schwerdtfeger, P. *J. Phys. Chem. Lett.* **2012**, *3*, 209–213.

[17] Lu, R.; Rao, D.; Lu, Z.; Qian, J.; Li, F.; Wu, H.; Wang, Y.; Xiao, C.; Deng, K.; Kan, E.; Deng, W. *J. Phys. Chem. C* **2012**, *116*, 21291–21296.

[18] Lu, R.; Meng, Z.; Kan, E.; Li, F.; Rao, D.; Lu, Z.; Qian, J.; Xiao, C.; Wu, H.; Deng, K. *Phys. Chem. Chem. Phys.* **2013**, *15*, 666–670.

[19] Brockway, A. M.; Schrier, J. *J. Phys. Chem. C* **2013**, *117*, 393–402.

[20] Lu, R.; Meng, Z.; Rao, D.; Wang, Y.; Shi, Q.; Zhang, Y.; Kan, E.; Xiao, C.; Deng, K. *Nanoscale* **2014**, *6*, 9960–9964.

[21] Britz, D. A.; Khlobystov, A. N. *Chem. Soc. Rev.* **2006**, *35*, 637–659.

[22] Kauffman, D. R.; Star, A. *Angew. Chem. Int. Ed.* **2008**, *47*, 6550–6570.

[23] Cao, D.; Zhang, X.; Chen, J.; Wang, W.; Yun, J. *J. Phys. Chem. B* **2003**, *107*, 13286–13292.

[24] Hirsch, A. *Angew. Chem. Int. Ed.* **2002**, *41*, 1853–1859.

[25] Herm, Z. R.; Swisher, J. A.; Smit, B.; Krishna, R.; Long, J. R. *J. Am. Chem. Soc.* **2011**, *133*, 5664–5667.

[26] Kowalczyk, P. *Phys. Chem. Chem. Phys.* **2012**, *14*, 2784–2790.

[27] Grimme, S. *J. Comput. Chem.* **2006**, *27*, 1787–1799.

[28] Becke, A. D.; Johnson, E. R. *J. Chem. Phys.* **2007**, *127*, 124108.

[29] Zhao, Y.; Truhlar, D. G. *Theor. Chem. Acc.* **2008**, *120*, 215–241.

[30] Chai, J.-D.; Head-Gordon, M. *Phys. Chem. Chem. Phys.* **2008**, *10*, 6615–6620.

[31] Tkatchenko, A.; Scheffler, M. *Phys. Rev. Lett.* **2009**, *102*, 073005.

[32] Pernal, K.; Podeszwa, R.; Patkowski, K.; Szalewicz, K. *Phys. Rev. Lett.* **2009**, *103*, 263201.

[33] Grimme, S.; Antony, J.; Ehrlich, S.; Krieg, H. *J. Chem. Phys.* **2010**, *132*, 154104.

[34] Vydrov, O. A.; Van Voorhis, T. *J. Chem. Phys.* **2010**, *133*, 244103.

[35] Jurečka, P.; Šponer, J.; Černý, J.; Hobza, P. *Phys. Chem. Chem. Phys.* **2006**, *8*, 1985–1993.

[36] Řezáč, J.; Riley, K. E.; Hobza, P. *J. Chem. Theory Comput.* **2011**, *7*, 2427–2438.

[37] Risthaus, T.; Grimme, S. *J. Chem. Theory Comput.* **2013**, *9*, 1580–1591.

[38] Burns, L. A.; Vazquez-Mayagoitia, A.; Sumpter, B. G.; Sherrill, C. D. *J. Chem. Phys.* **2011**, *134*, 084107.

[39] Smith, D. G. A.; Patkowski, K. *J. Chem. Theory Comput.* **2013**, *9*, 370–389.

[40] Smith, D. G. A.; Patkowski, K. *J. Phys. Chem. C* **2014**, *118*, 544–550.

[41] Smith, D. G. A.; Patkowski, K. *J. Phys. Chem. C* **2015**, *119*, 4934–4948.

[42] Vogiatzis, K. D.; Mavrandonakis, A.; Klopper, W.; Froudakis, G. E. *ChemPhysChem* **2009**, *10*, 374–383.

[43] Mackie, I. D.; DiLabio, G. A. *Phys. Chem. Chem. Phys.* **2011**, *13*, 2780–2787.

[44] Schütz, M.; Manby, F. R. *Phys. Chem. Chem. Phys.* **2003**, *5*, 3349–3358.

[45] Voloshina, E.; Usvyat, D.; Schütz, M.; Dedkov, Y.; Paulus, B. *Phys. Chem. Chem. Phys.* **2011**, *13*, 12041–12047.

[46] Schütz, M.; Yang, J.; Chan, G. K.; Manby, F. R.; Werner, H.-J. *J. Chem. Phys.* **2013**, *138*, 054109.

[47] Riplinger, C.; Sandhoefer, B.; Hansen, A.; Neese, F. *J. Chem. Phys.* **2013**, *139*, 134101.

[48] Werner, H.-J. et al. MOLPRO, version 2012.1, a package of ab initio programs. 2012; see http://www.molpro.net (accessed June 2, 2014).

[49] Werner, H.; Manby, F. R.; Knowles, P. J. *J. Chem. Phys.* **2003**, *118*, 8149–8160.

[50] Dunning Jr., T. H. *J. Chem. Phys.* **1989**, *90*, 1007–1023.

[51] Kendall, R. A.; Dunning Jr., T. H.; Harrison, R. J. *J. Chem. Phys.* **1992**, *96*, 6796–6806.

[52] Hättig, C. *Phys. Chem. Chem. Phys.* **2005**, *7*, 59–66.

[53] Weigend, F.; Köhn, A.; Hättig, C. *J. Chem. Phys.* **2002**, *116*, 3175–3183.

[54] Boys, S. F.; Bernardi, F. *Mol. Phys.* **1970**, *19*, 553–566.

[55] van Duijneveldt, F. B.; van Duijneveldt-van de Rijdt, J. G. C. M.; van Lenthe, J. H. *Chem. Rev.* **1994**, *94*, 1873–1885.

[56] Sinnokrot, M. O.; Sherrill, C. D. *J. Phys. Chem. A* **2004**, *108*, 10200–10207.

[57] Halkier, A.; Helgaker, T.; Jørgensen, P.; Klopper, W.; Koch, H.; Olsen, J.; Wilson, A. K. *Chem. Phys. Lett.* **1998**, *286*, 243–252.

[58] Hill, J. G.; Peterson, K. A.; Knizia, G.; Werner, H.-J. *J. Chem. Phys.* **2009**, *131*, 194105.

[59] Patkowski, K. *J. Chem. Phys.* **2012**, *137*, 034103.

[60] Adler, T. B.; Knizia, G.; Werner, H.-J. *J. Chem. Phys.* **2007**, *127*, 221106.

[61] Knizia, G.; Adler, T. B.; Werner, H.-J. *J. Chem. Phys.* **2009**, *130*, 054104.

[62] Köhn, A. *J. Chem. Phys.* **2009**, *130*, 131101.

[63] Marchetti, O.; Werner, H.-J. *Phys. Chem. Chem. Phys.* **2008**, *10*, 3400–3409.

[64] Tew, D. P.; Klopper, W.; Hättig, C. *Chem. Phys. Lett.* **2008**, *452*, 326–332.

[65] Marchetti, O.; Werner, H.-J. *J. Phys. Chem. A* **2009**, *113*, 11580–11585.

[66] Zhao, Y.; Truhlar, D. G. *J. Phys. Chem. A* **2006**, *110*, 5121–5129.

[67] Becke, A. D. *J. Chem. Phys.* **1993**, *98*, 5648–5652.

[68] Stephens, P. J.; Devlin, F. J.; Chabalowski, C. F.; Frisch, M. J. *J. Phys. Chem.* **1994**, *98*, 11623–11627.

[69] Becke, A. D. *Phys. Rev. A* **1988**, *38*, 3098–3100.

[70] Perdew, J. P.; Burke, K.; Ernzerhof, M. *Phys. Rev. Lett.* **1996**, *77*, 3865–3868.

[71] Adamo, C.; Barone, V. *J. Chem. Phys.* **1999**, *110*, 6158–6170.

[72] Ernzerhof, M.; Scuseria, G. E. *J. Chem. Phys.* **1999**, *110*, 5029–5036.

[73] Vydrov, O. A.; Scuseria, G. E. *J. Chem. Phys.* **2006**, *125*, 234109.

[74] Grimme, S.; Ehrlich, S.; Goerigk, L. *J. Comput. Chem.* **2011**, *32*, 1456–1465.

[75] Grimme, S. *J. Chem. Phys.* **2006**, *124*, 034108.

[76] Johnson, E. R.; Becke, A. D.; Sherrill, C. D.; DiLabio, G. A. *J. Chem. Phys.* **2009**, *131*, 034111.

[77] Wheeler, S. E.; Houk, K. N. *J. Chem. Theory Comput.* **2010**, *6*, 395–404.

[78] Weigend, F. *Phys. Chem. Chem. Phys.* **2002**, *4*, 4285–4291.

[79] Turney, J. M. et al. *WIREs Comput Mol Sci* **2012**, *2*, 556–565.

[80] Papajak, E.; Zheng, J.; Xu, X.; Leverentz, H. R.; Truhlar, D. G. *J. Chem. Theory Comput.* **2011**, *7*, 3027–3034.

[81] Grimme, S. *J. Chem. Phys.* **2003**, *118*, 9095–9102.

[82] Smith, D. G. A.; Jankowski, P.; Slawik, M.; Witek, H. A.; Patkowski, K. *J. Chem. Theory Comput.* **2014**, *10*, 3140–3150.

[83] Demovičová, L.; Hobza, P.; Řezáč, J. *Phys. Chem. Chem. Phys.* **2014**, *16*, 19115–19121.

[84] Pitoňak, M.; Neogrády, P.; Řezáč, J.; Jurečka, P.; Urban, M.; Hobza, P. *J. Chem. Theory Comput.* **2008**, *4*, 1829–1834.

[85] Kucharski, S. A.; Bartlett, R. J. *J. Chem. Phys.* **1998**, *108*, 9221–9226.

[86] Weigend, F.; Ahlrichs, R. *Phys. Chem. Chem. Phys.* **2005**, *7*, 3297–3305.

[87] Mardirossian, N.; Head-Gordon, M. *J. Chem. Phys.* **2014**, *140*, 18A527.

[88] Steinmann, S. N.; Wodrich, M. D.; Corminboeuf, C. *Theor. Chem. Acc.* **2010**, *127*, 429–442.

[89] Seth, M.; Ziegler, T.; Steinmetz, M.; Grimme, S. *J. Chem. Theory Comput.* **2013**, *9*, 2286–2299.

[90] Leininger, T.; Stoll, H.; Werner, H.-J.; Savin, A. *Chem. Phys. Lett.* **1997**, *275*, 151–160.

[91] Tawada, Y.; Tsuneda, T.; Yanagisawa, S.; Yanai, T.; Hirao, K. *J. Chem. Phys.* **2004**, *120*, 8425–8433.

[92] Gerber, I. C.; Ángyán, J. G. *Chem. Phys. Lett.* **2005**, *415*, 100–105.

[93] Tang, K. T.; Toennies, J. P. *J. Chem. Phys.* **1984**, *80*, 3726–3741.

[94] Gráfová, L.; Pitoňák, M.; Řezáč, J.; Hobza, P. *J. Chem. Theory Comput.* **2010**, *6*, 2365–2376.

[95] Gobre, V. V.; Tkatchenko, A. *Nature Comm.* **2013**, *4*, 2341.

[96] Misquitta, A. J.; Spencer, J.; Stone, A. J.; Alavi, A. *Phys. Rev. B* **2010**, *82*, 075312.

[97] Dobson, J. F. *Surf. Sci.* **2011**, *605*, 1621–1632.

[98] Tkatchenko, A.; DiStasio, Jr., R. A.; Car, R.; Scheffler, M. *Phys. Rev. Lett.* **2012**, *108*, 236402.

TABLE I. The MP2 and ΔCCSD(T) interaction energy contributions (in kcal/mol) for the lowest-energy structures of the pyrazine-CO_2 and quinoxaline–CO_2 complexes. The rows marked "ext." display the CBS-extrapolated results — the value in the aXZ column was obtained from the $(X-1, X)$ extrapolation.

	in-plane pyrazine-CO_2				stacked pyrazine-CO_2				in-plane quinoxaline-CO_2				stacked quinoxaline-CO_2			
method	aDZ	aTZ	aQZ	a5Z	aDZ	aTZ	aQZ	a5Z	aDZ	aTZ	aQZ	a5Z	aDZ	aTZ	aQZ	a5Z
MP2	-3.328	-3.667	-3.786	-3.838	-1.208	-1.544	-1.631	-1.672	-3.837	-4.221	-4.361	-4.420	-3.296	-3.765	-3.920	-3.987
ext.		-3.811	-3.871	-3.886		-1.686	-1.698	-1.711		-4.388	-4.459	-4.474		-3.969	-4.032	-4.051
MP2-F12	-3.851	-3.902	-3.893	-3.896	-1.635	-1.696	-1.705	-1.711	-4.439	-4.481	-4.481	-4.482	-3.985	-4.029	-4.043	-4.055
ext.		-3.925	-3.888	-3.898		-1.722	-1.712	-1.717		-4.501	-4.482	-4.483		-4.048	-4.053	-4.068
ΔCCSD(T)	0.082	0.043	0.037		0.468	0.503	0.518		0.113	0.071			1.097	1.139		
ext.		0.026	0.032			0.517	0.528			0.054				1.157		
ΔCCSD(T)-F12a	0.104	0.069	0.054		0.521	0.534	0.536		0.140	0.103			1.188	1.192		
ext.		0.054	0.044			0.540	0.537			0.087				1.194		
ΔCCSD(T**)-F12a	0.011	0.033	0.038		0.374	0.480	0.511		0.018	0.057			0.947	1.104		
ext.		0.043	0.041			0.525	0.533			0.073				1.170		
ΔCCSD(T)-F12b	0.198	0.107	0.075		0.644	0.580	0.557		0.254	0.148			1.400	1.270		
ext.		0.069	0.051			0.554	0.540			0.104				1.215		
ΔCCSD(T**)-F12b	0.105	0.071	0.058		0.496	0.526	0.532		0.131	0.102			1.159	1.182		
ext.		0.058	0.049			0.538	0.536			0.090				1.191		
ΔCCSD(T)-F12avg	0.104	0.070	0.056		0.509	0.530	0.534		0.135	0.102			1.173	1.187		
ext.		0.056	0.046			0.539	0.537			0.088				1.193		
CCSD(T)/aXZ	-3.245	-3.623	-3.755		-0.735	-1.040	-1.118		-3.723	-4.149			-2.192	-2.624		
CCSD(T)/$(X-1, X)$		-3.782	-3.850			-1.168	-1.174			-4.328				-2.806		
CCSD(T)-F12avg/aXZ	-3.747	-3.832	-3.837		-1.126	-1.166	-1.172		-4.303	-4.379			-2.811	-2.842		
CCSD(T)-F12avg/$(X-1, X)$		-3.868	-3.841			-1.183	-1.175			-4.411				-2.855		
MP2/(Q,5)+ ΔCCSD(T)/aXZ	-3.804	-3.843	-3.850		-1.243	-1.209	-1.194		-4.361	-4.403			-2.955	-2.911		
MP2/(Q,5)+ ΔCCSD(T)/$(X-1, X)$		-3.860	-3.854			-1.194	-1.183			-4.420				-2.894		
MP2/(Q,5)+ ΔCCSD(T)-F12avg/aXZ	-3.782	-3.816	-3.830		-1.203	-1.181	-1.178		-4.339	-4.372			-2.878	-2.864		
MP2/(Q,5)+ ΔCCSD(T)-F12avg/$(X-1, X)$		-3.830	-3.840			-1.172	-1.175			-4.386				-2.859		
MP2-F12/(Q,5)+ ΔCCSD(T)-F12avg/aXZ	-3.794	-3.828	-3.842		-1.208	-1.187	-1.183		-4.347	-4.381			-2.894	-2.881		
MP2-F12/(Q,5)+ ΔCCSD(T)-F12avg/$(X-1, X)$		-3.842	-3.852			-1.177	-1.180			-4.394				-2.876		

TABLE II. The MP2 and ΔCCSD(T) contributions to the in-plane and stacked 2-azapyrene-CO_2 and 1,6-diazacoronene-CO_2 interaction energies (in kcal/mol) as functions of $\eta = z/z_{\min}$. No density fitting was used in this table.

		2-azapyrene–CO_2				1,6-diazacoronene–CO_2			
		MP2		ΔCCSD(T)		MP2		ΔCCSD(T)	
basis	η	in-plane	stacked	in-plane	stacked	in-plane	stacked	in-plane	stacked
cc-pVDZ	0.8	7.093	12.359	0.300	3.484	7.992	12.241	0.483	3.670
	0.9	-0.251	1.555	0.090	2.028	-0.363	1.183	0.179	2.236
	1.0	-2.322	-1.405	0.005	1.218	-2.587	-1.929	0.053	1.396
	1.2	-2.087	-1.525	-0.013	0.498	-2.215	-2.001	0.007	0.600
	1.4	-1.222	-0.854	-0.001	0.233	-1.258	-1.180	0.010	0.287
	1.6	-0.691	-0.462	0.002	0.118	-0.695	-0.675	0.009	0.147
laDZ	0.8	3.986	8.005	0.386	4.093	4.962	7.440	0.583	4.380
	0.9	-2.365	-1.533	0.139	2.447	-2.442	-2.321	0.230	2.759
	1.0	-3.855	-3.581	0.026	1.499	-4.089	-4.479	0.080	1.768
	1.2	-2.878	-2.541	-0.012	0.621	-3.039	-3.264	0.014	0.781
	1.4	-1.657	-1.320	0.001	0.292	-1.714	-1.793	0.015	0.382
	1.6	-0.956	-0.692	0.008	0.151	-0.957	-0.991	0.016	0.201
aDZ	0.8	4.005	7.595	0.366	4.085	4.811	6.955		
	0.9	-2.369	-1.777	0.119	2.441	-2.540	-2.644		
	1.0	-3.826	-3.723	0.015	1.493	-4.151	-4.695		
	1.2	-2.906	-2.584	-0.018	0.615	-3.109	-3.337		
	1.4	-1.678	-1.331	-0.004	0.288	-1.721	-1.812		
	1.6	-0.943	-0.691	0.005	0.147	-0.975	-0.993		

TABLE III. The optimized minimum distance $z_{\min}$ (Å), the O-C-O angle deformation $\Delta\phi_{\mathrm{OCO}}$ (°), the CO_2-only flexible energy change ΔE_{flex} (kcal/mol), and the C-O bond length change Δr_{CO} (Å), calculated at the MP2/aTZ level for the lowest-energy N-PHAC–CO_2 structures. The N-PHAC monomer was kept rigid.

Complex	Orientation	z_{min}	$\Delta\phi_{\mathrm{OCO}}$	ΔE_{flex}	Δr_{CO}
pyridine-CO_2	in-plane	2.826	3.15	0.166	0.0003
	stacked	3.144	0.75	0.011	0.0011
pyrazine-CO_2	in-plane	2.840	2.58	0.112	0.0002
	stacked	3.370	0.13	0.001	0.0004
quinoline-CO_2	in-plane	2.846	2.97	0.148	0.0003
	stacked	3.138	0.73	0.011	0.0013
quinoxaline-CO_2	in-plane	2.873	2.61	0.114	0.0002
	stacked	3.080	0.31	0.003	0.0010
pyrido[3,2-g]quinoline-CO_2	in-plane	2.883	2.80	0.132	0.0008
	stacked	3.103	0.47	0.006	0.0015
phenanthroline-CO_2	in-plane	3.791	3.93	0.258	0.0004
	stacked	2.821	3.56	0.215	0.0014
2-azapyrene-CO_2	in-plane	2.813	3.30	0.183	0.0004
	stacked	3.139	0.41	0.005	0.0014

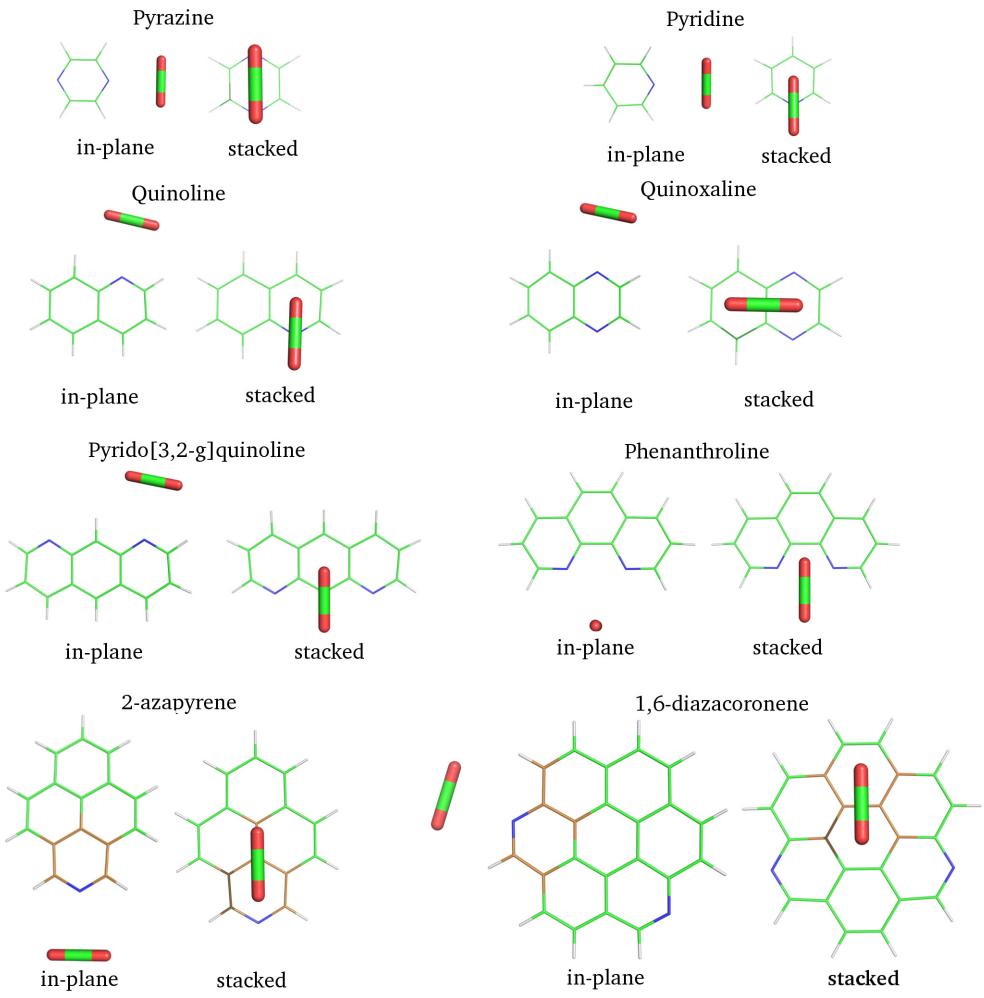

FIG. 1. The structures of the model CO_2–N-PHAC complexes. The in-plane configurations represent the global minima, "stacked" are the related 3D stacked structures. The bronze-colored carbon atoms in the N-PHAC molecule as well as the closest nitrogen atom (blue) are those that have diffuse functions in the laDZ basis.

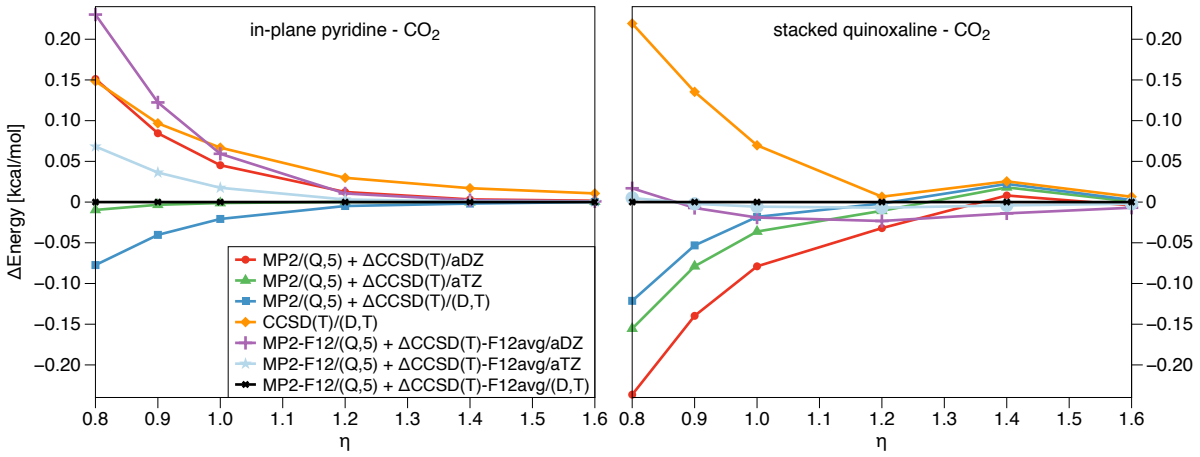

FIG. 2. Differences between the benchmark MP2-F12/(Q,5) + ΔCCSD(T)-F12avg/(D,T) interaction energy and other CCSD(T)/CBS schemes as functions of η for the in-plane pyridine-CO_2 (left panel) and stacked quinoxaline-CO_2 (right panel) complexes.

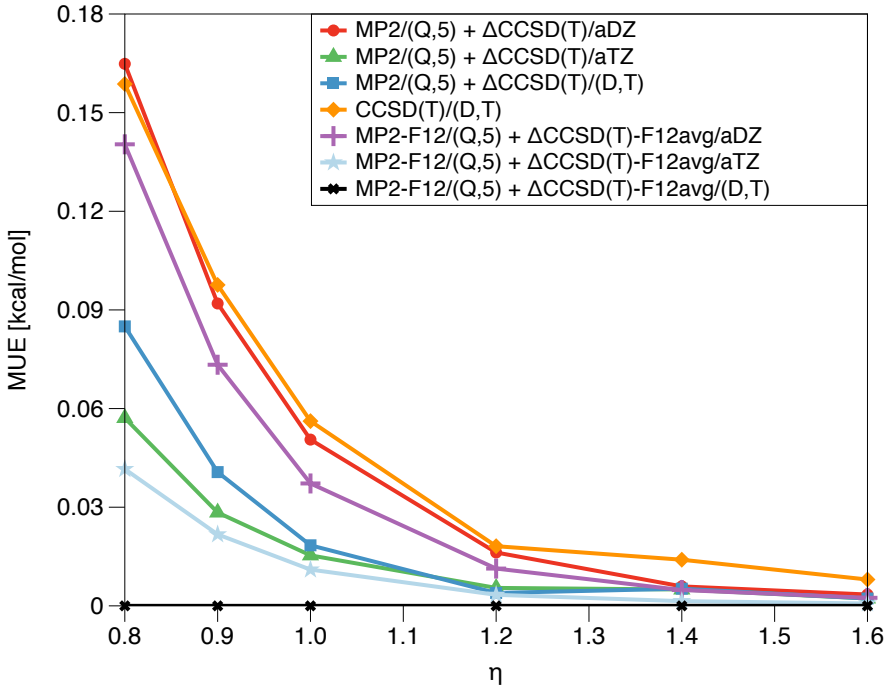

FIG. 3. The mean unsigned error (MUE) for different CCSD(T)/CBS estimates as a function of η, using the MP2-F12/(Q,5)+ΔCCSD(T)-F12avg/(D,T) as the benchmark interaction energy for the seven symmetric 1- and 2-ring systems.

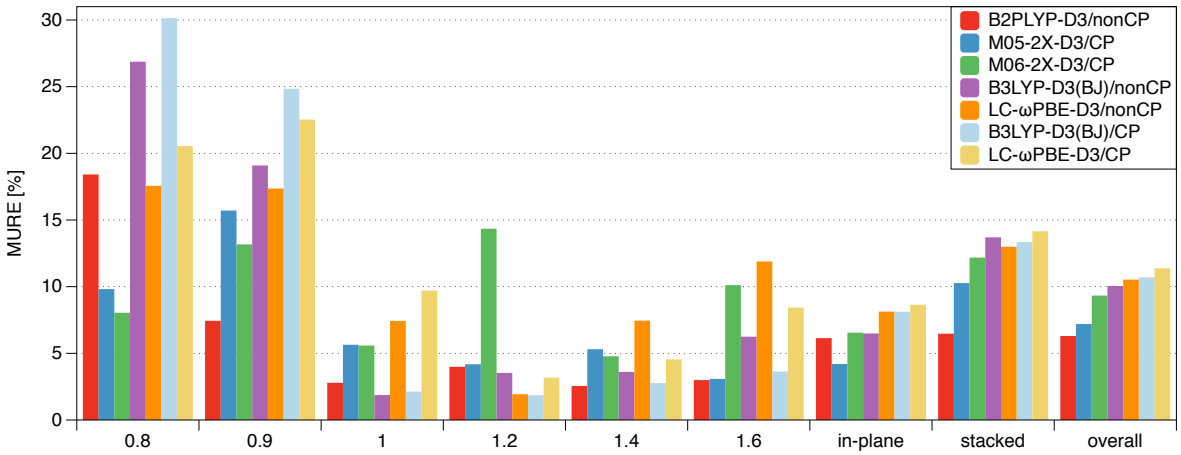

FIG. 4. Mean unsigned relative errors (MURE) for the best-performing DFT-based methods in the QZVP basis set as functions of the relative intermolecular separation η (the overall value for all η is displayed as "Overall") compared against the MP2/CBS+ΔCCSD(T) benchmark interaction energies for the 95 model N-PHAC-CO_2 geometries. In addition, separate MURE values for the in-plane and stacked structures are displayed.

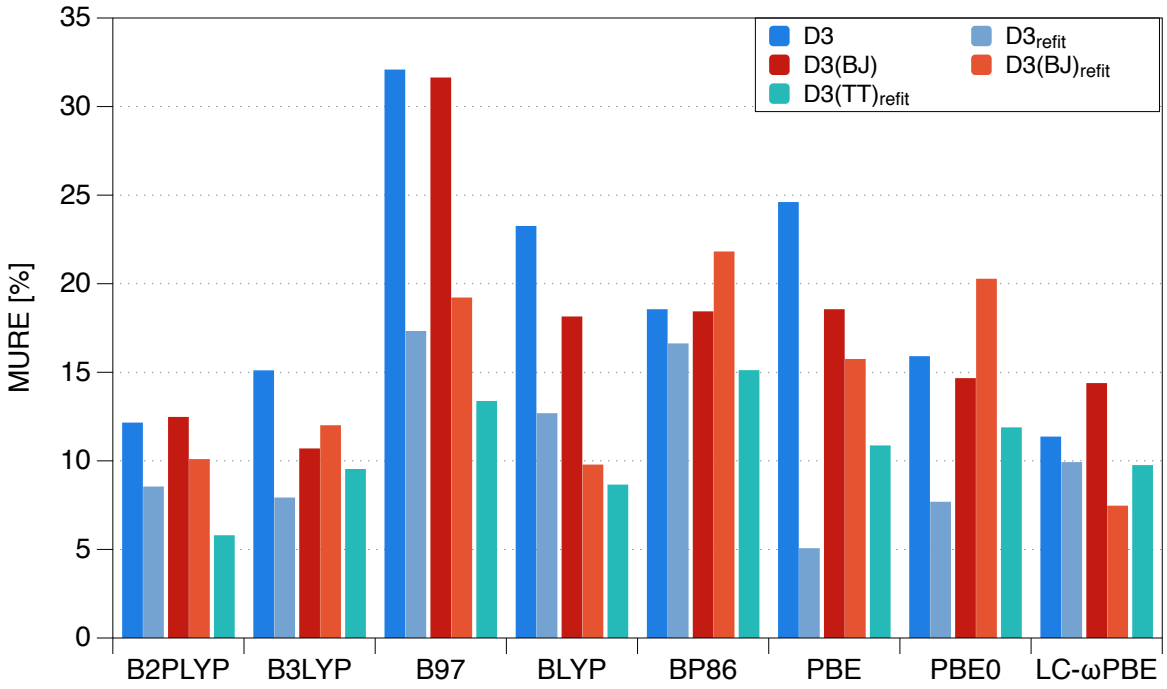

FIG. 5. Mean unsigned relative errors (MURE) for CP-corrected DFT-D3 interaction energies using different damping functions (original and refitted in Ref. 41) in the largest basis set QZVP, against the MP2/CBS+ΔCCSD(T) benchmark interaction energies for the 95 model N-PHAC-CO_2 geometries.

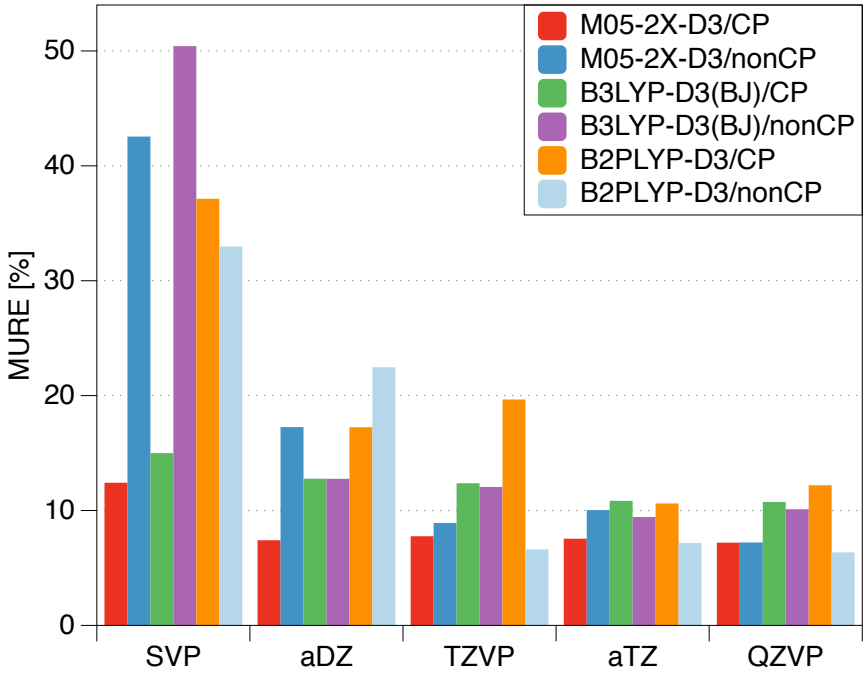

FIG. 6. Mean unsigned relative errors (MURE) for the best performers: M05-2X-D3, B2PLYP-D3, and B3LYP-D3(BJ) in different basis sets, with and without the CP correction, against the MP2/CBS+ΔCCSD(T) benchmark interaction energies for the 95 model N-PHAC-CO_2 geometries.

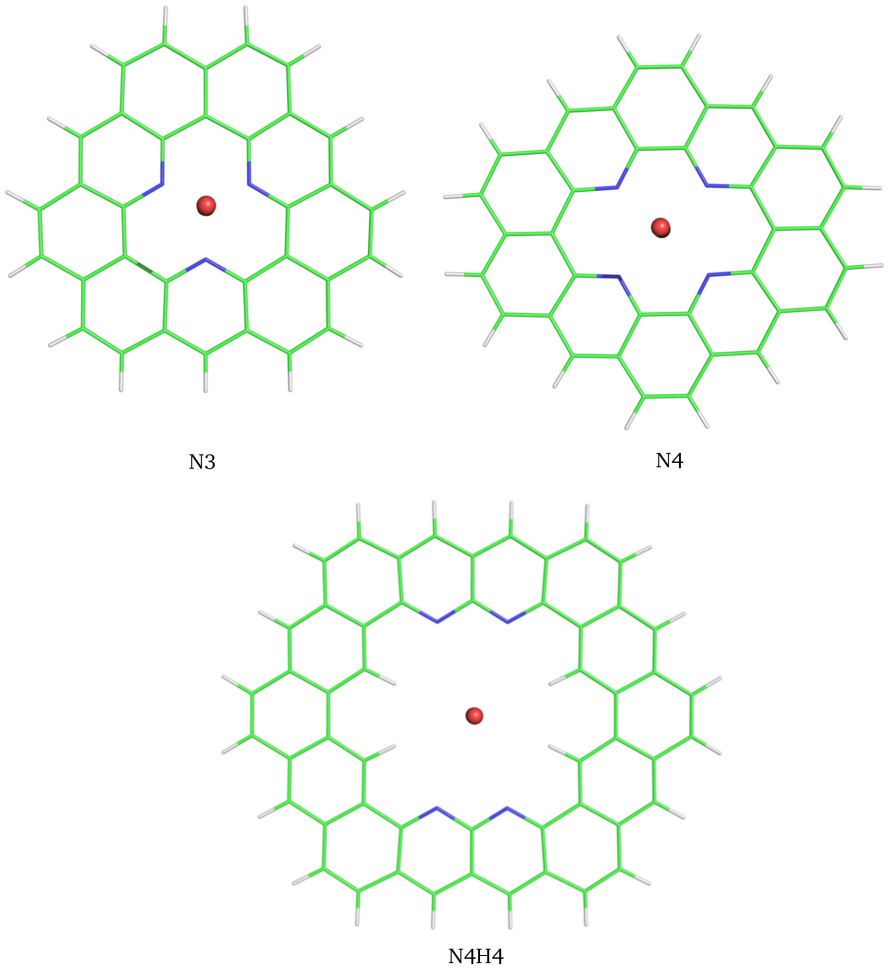

FIG. 7. The structures for CO_2 interacting with the N-PHAC models of the N3, N4, and N4H4 vacancies in N-doped graphene.

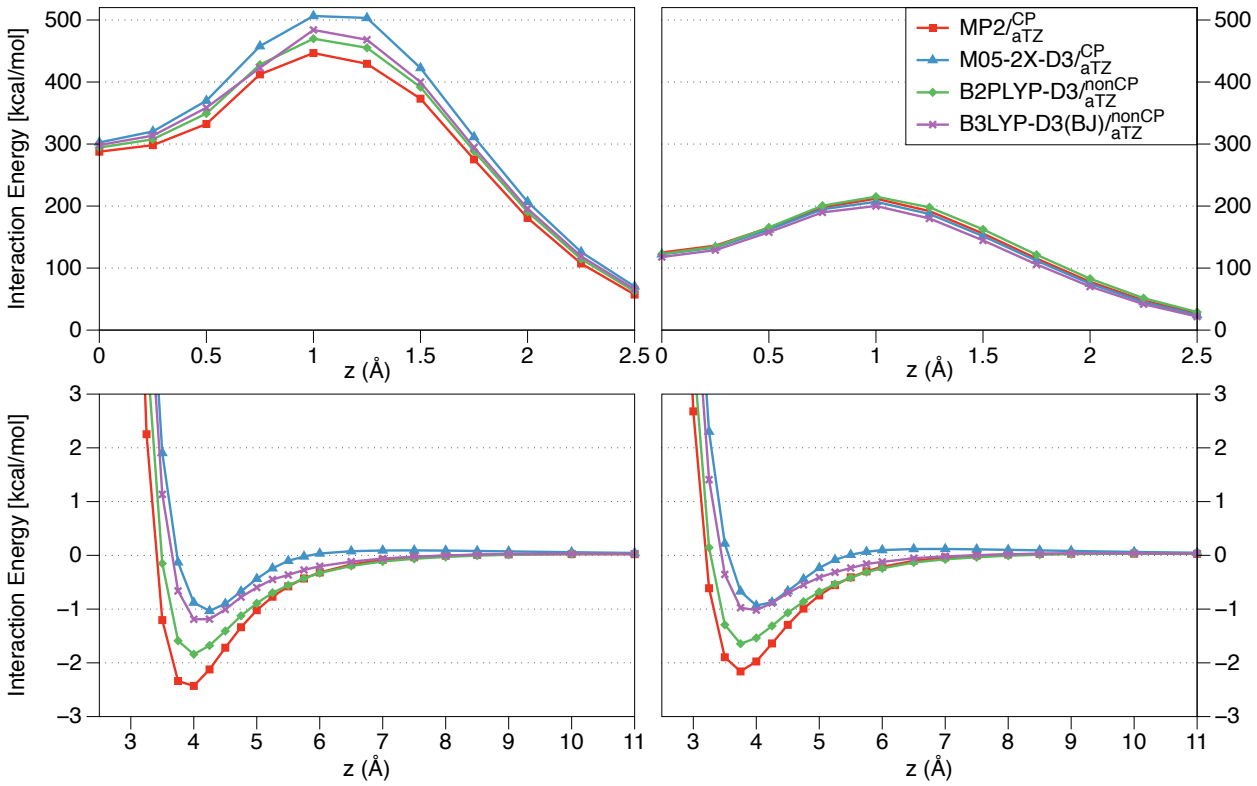

FIG. 8. MP2 and DFT+D interaction energies (in kcal/mol) for the N3 vacancy–CO_2 (left panels) and N4 vacancy–CO_2 (right panels) complexes as functions of the distance z from the CO_2 carbon to the N-PHAC plane. The upper panels display interaction energies at the repulsive region while the lower panels show interaction energies at the minimum and long-range distances. The CO_2 molecule is located along the symmetry axis perpendicular to the N-PHAC plane as illustrated in Fig. 7. The interacting molecules are kept rigid.

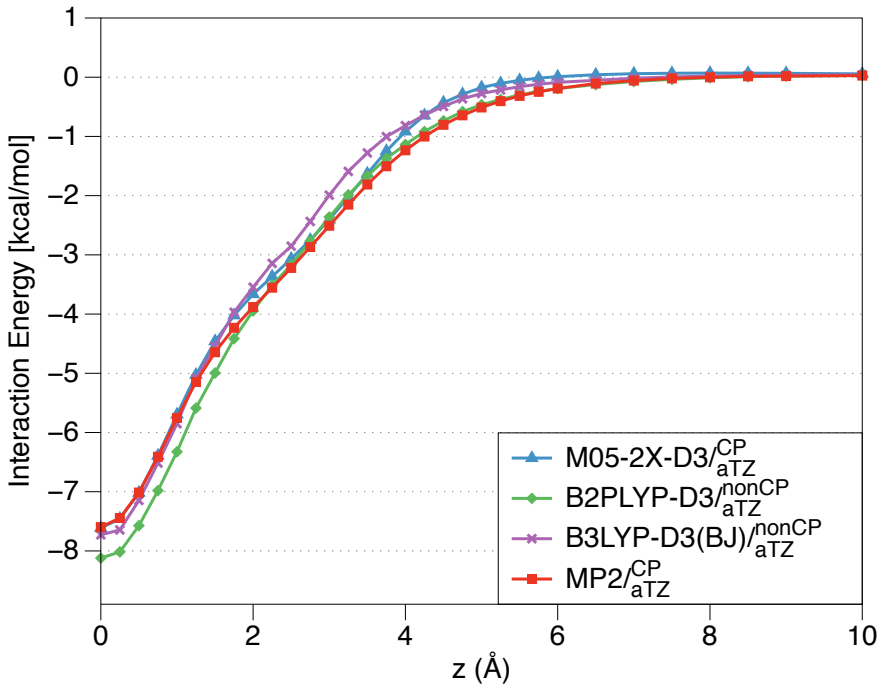

FIG. 9. MP2 and DFT+D interaction energies (in kcal/mol) for the N4H4 vacancy–CO_2 complexes as functions of the distance z from the CO_2 carbon to the N-PHAC plane. The CO_2 molecule is located along the symmetry axis perpendicular to the N-PHAC plane as illustrated in Fig. 7.

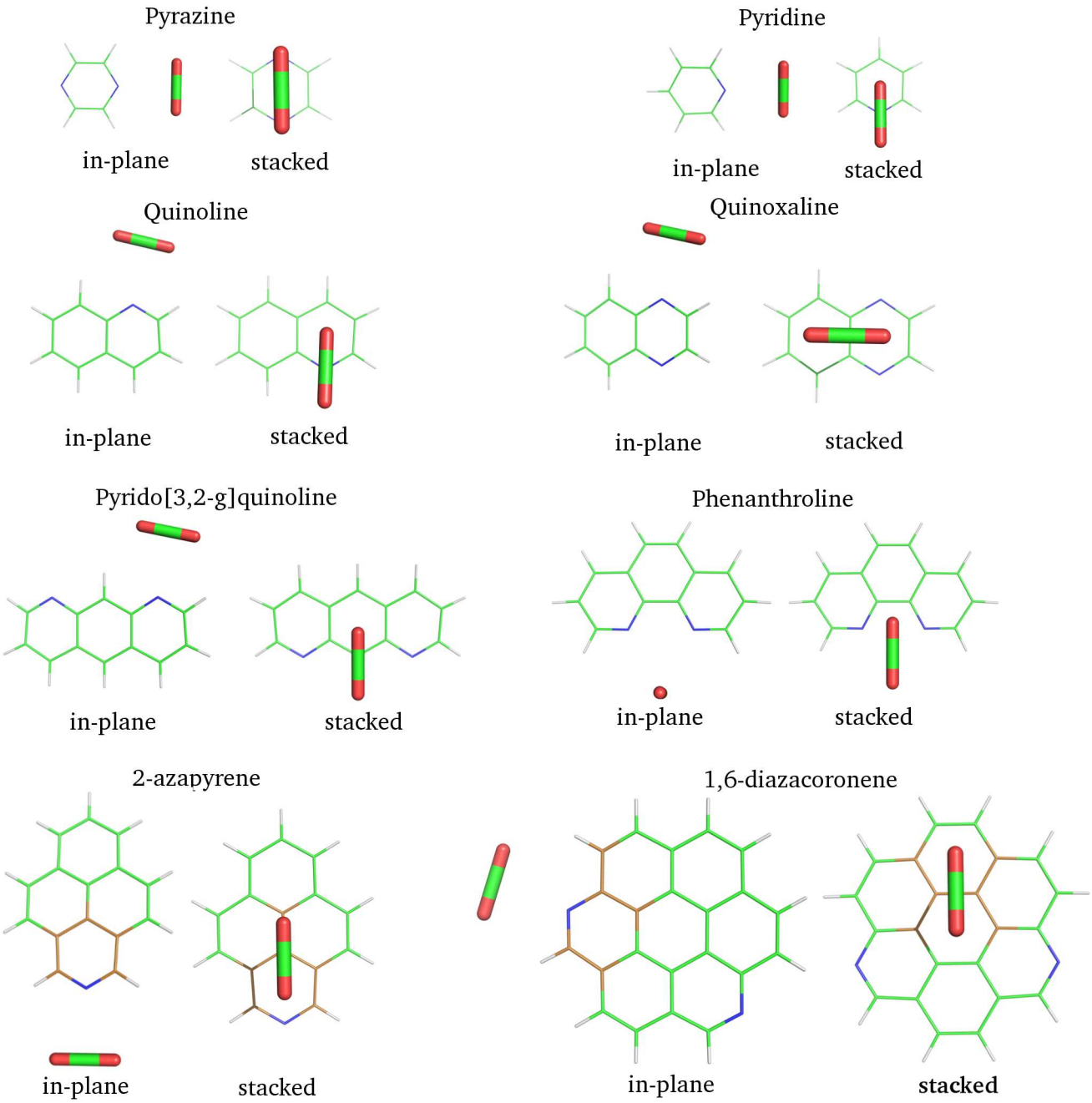

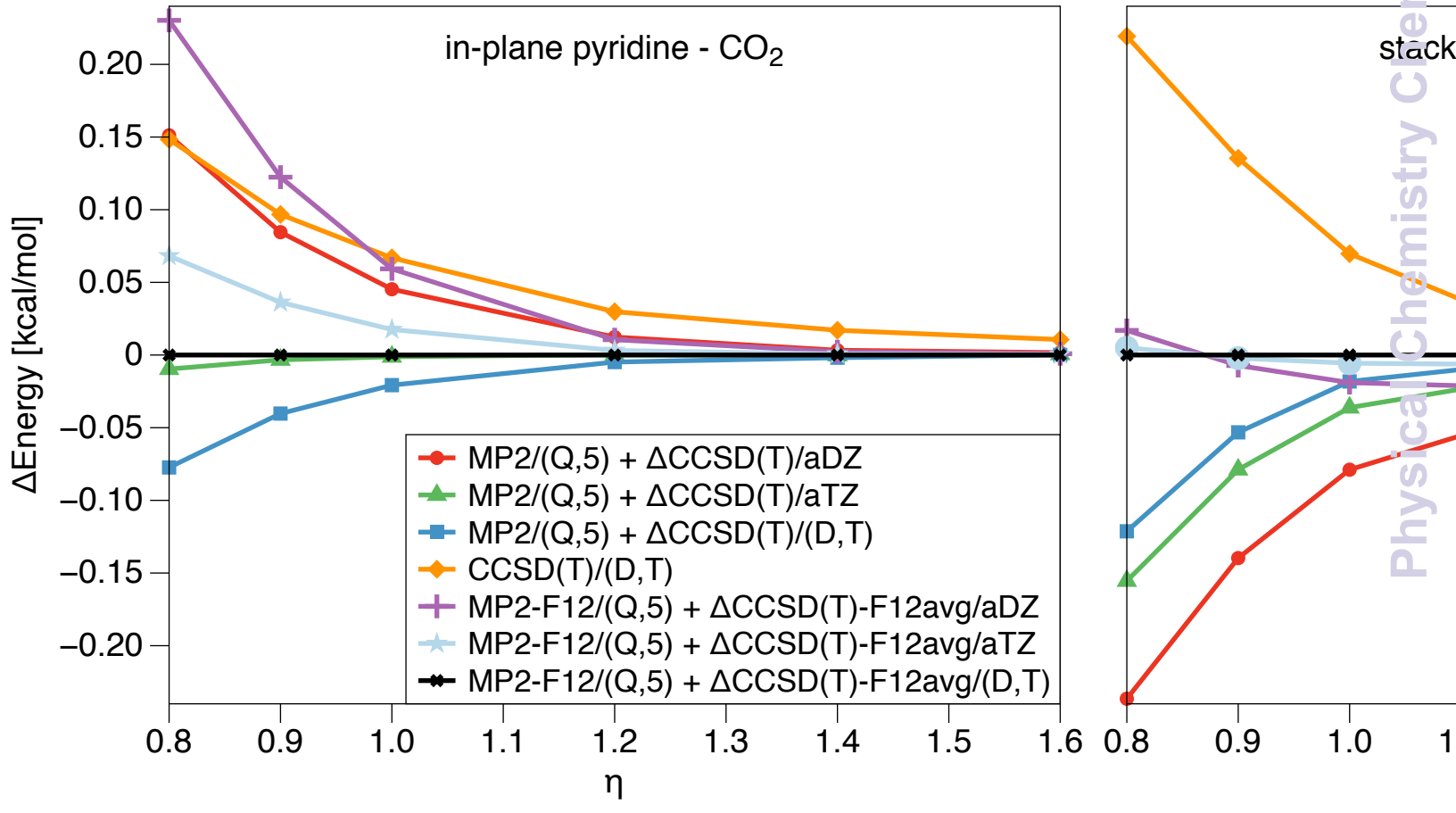

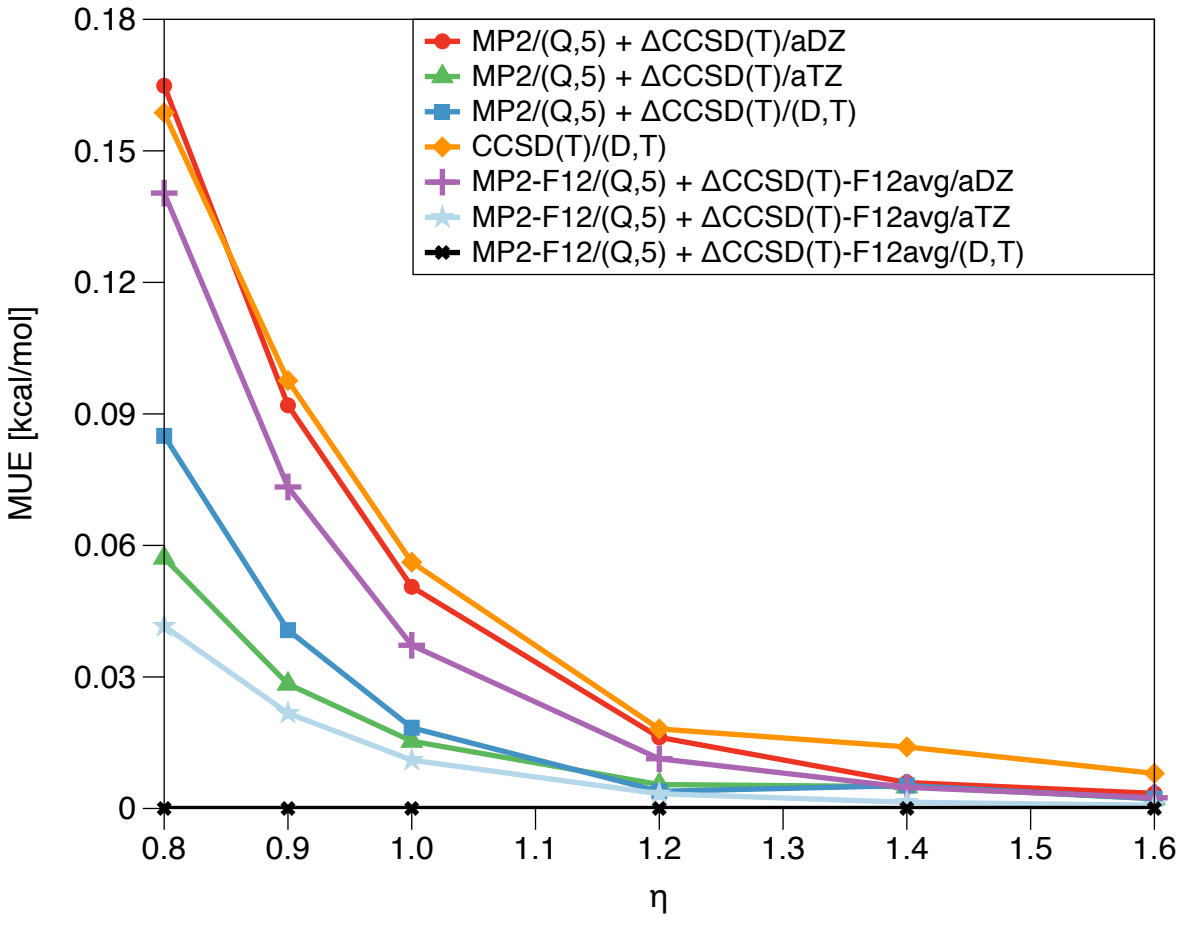

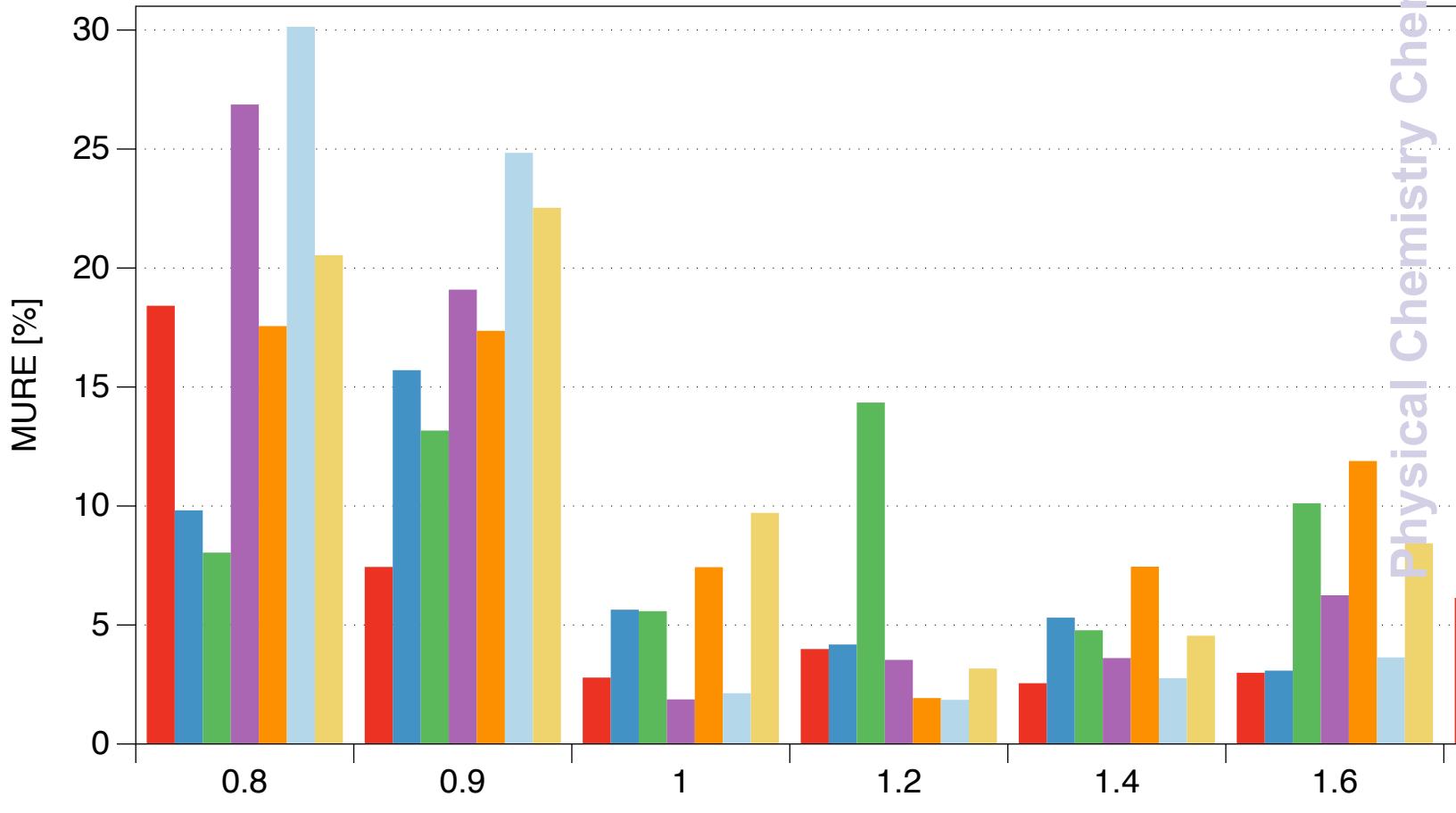

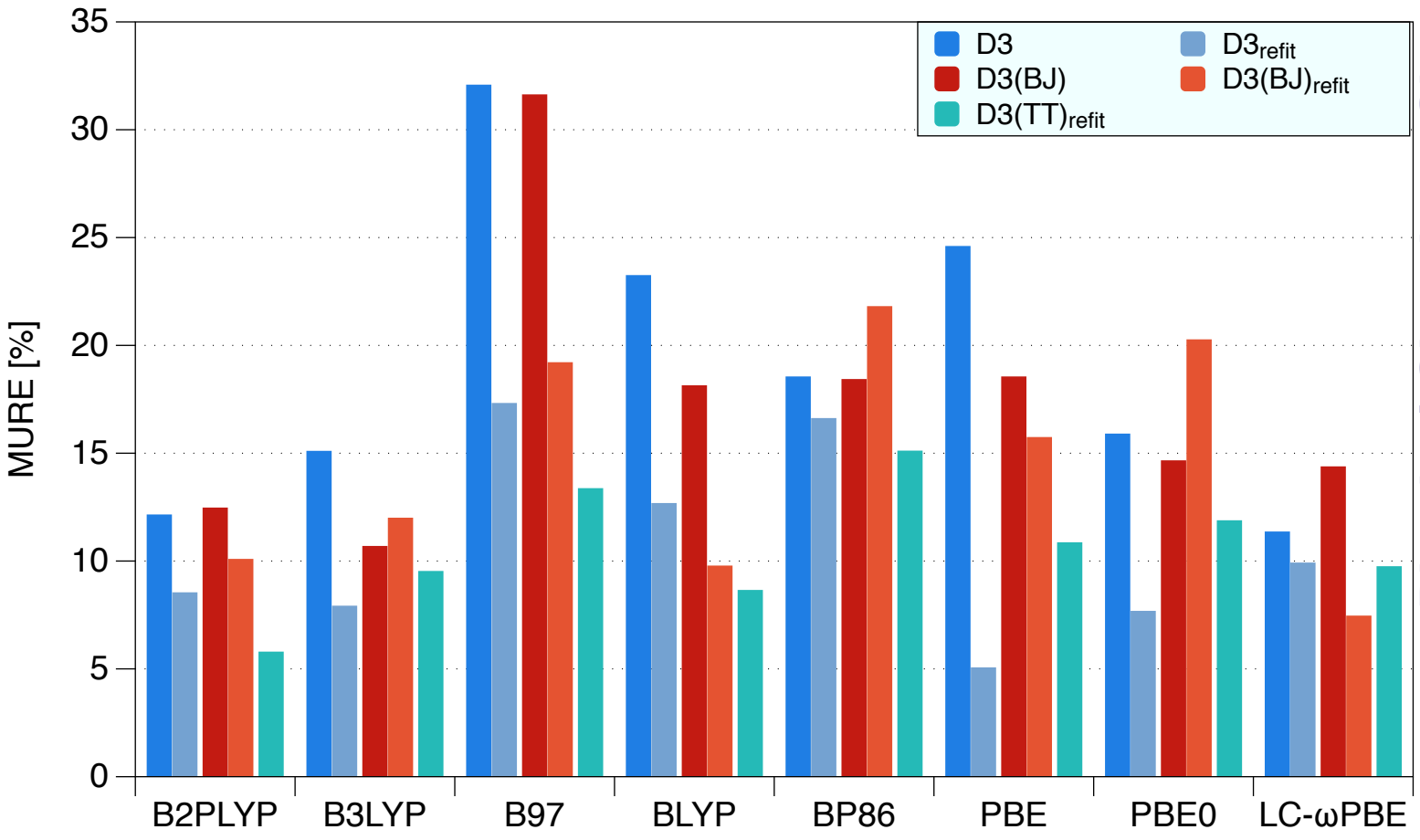

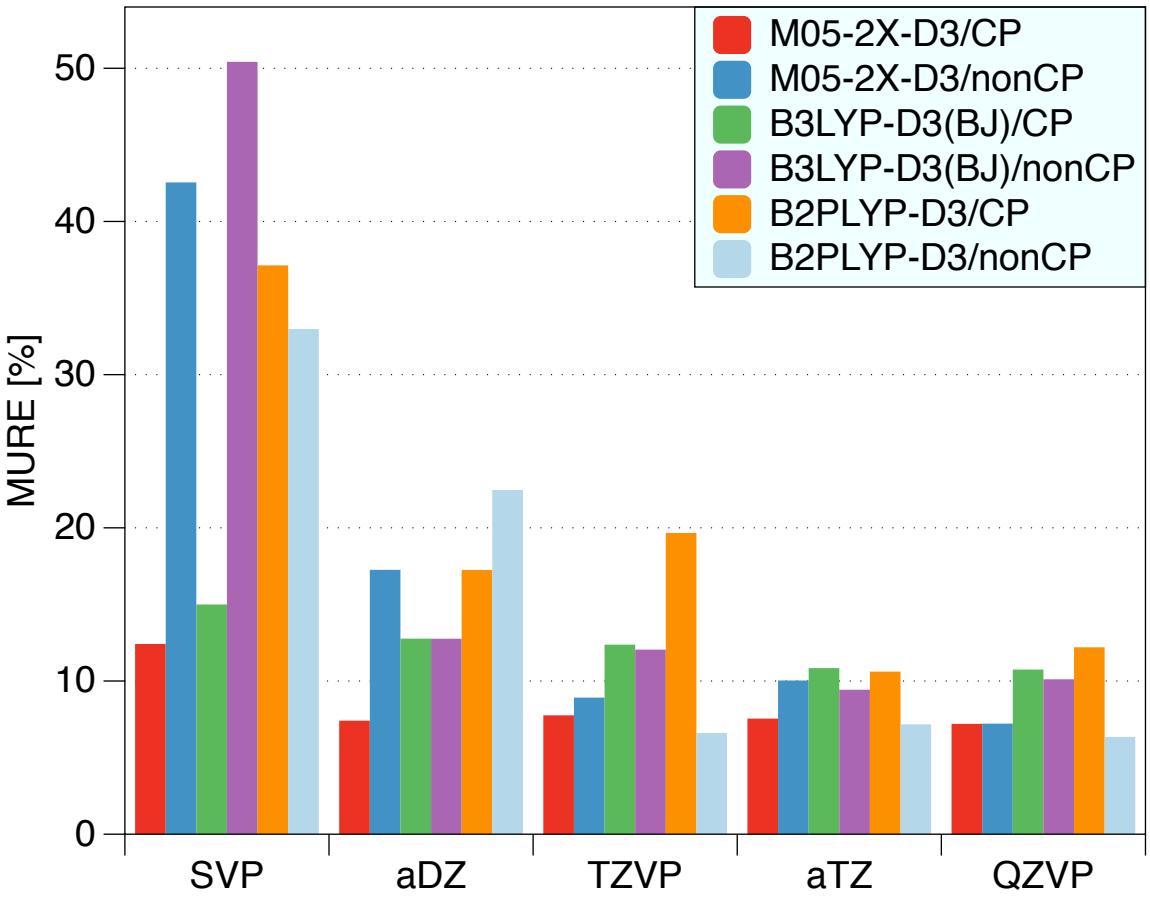

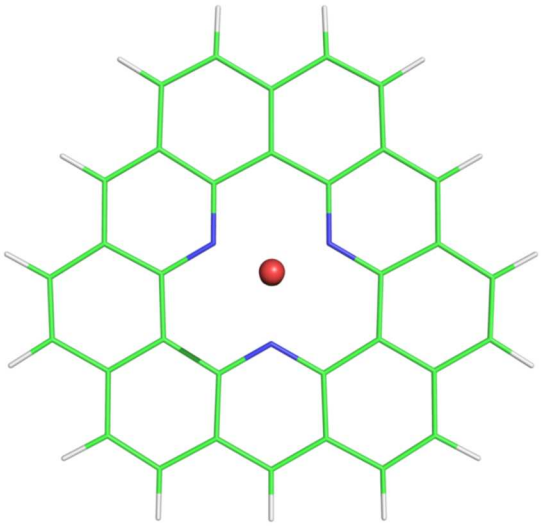

N3

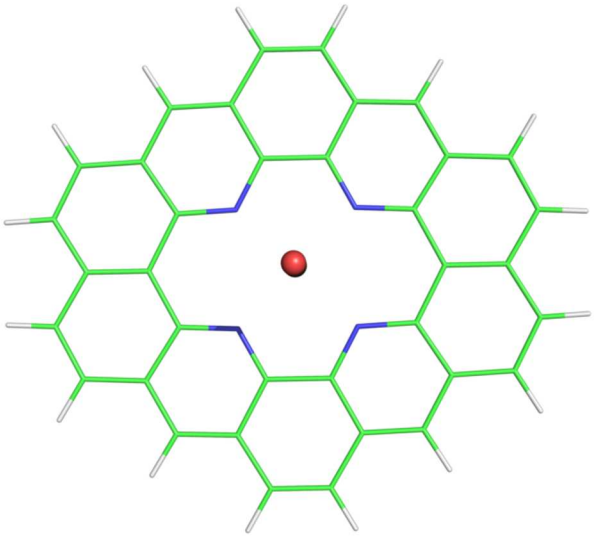

N4

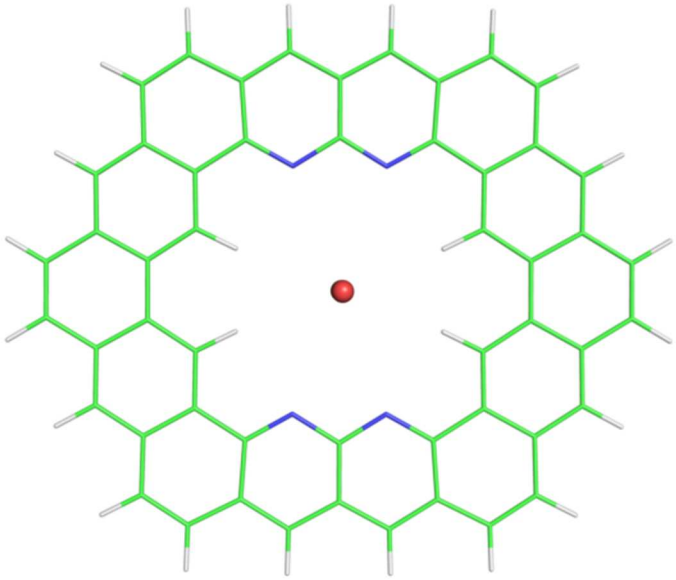

N4H4

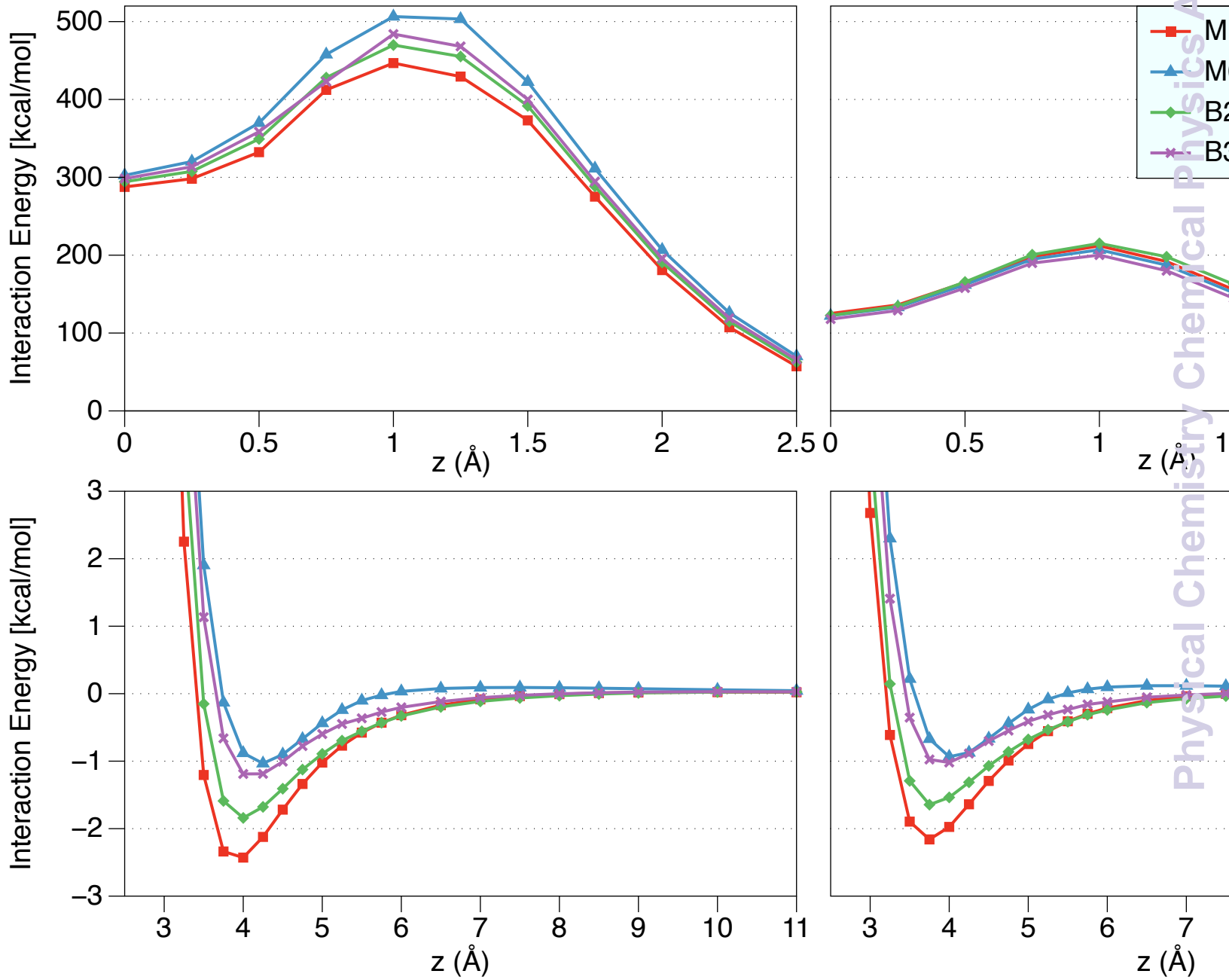

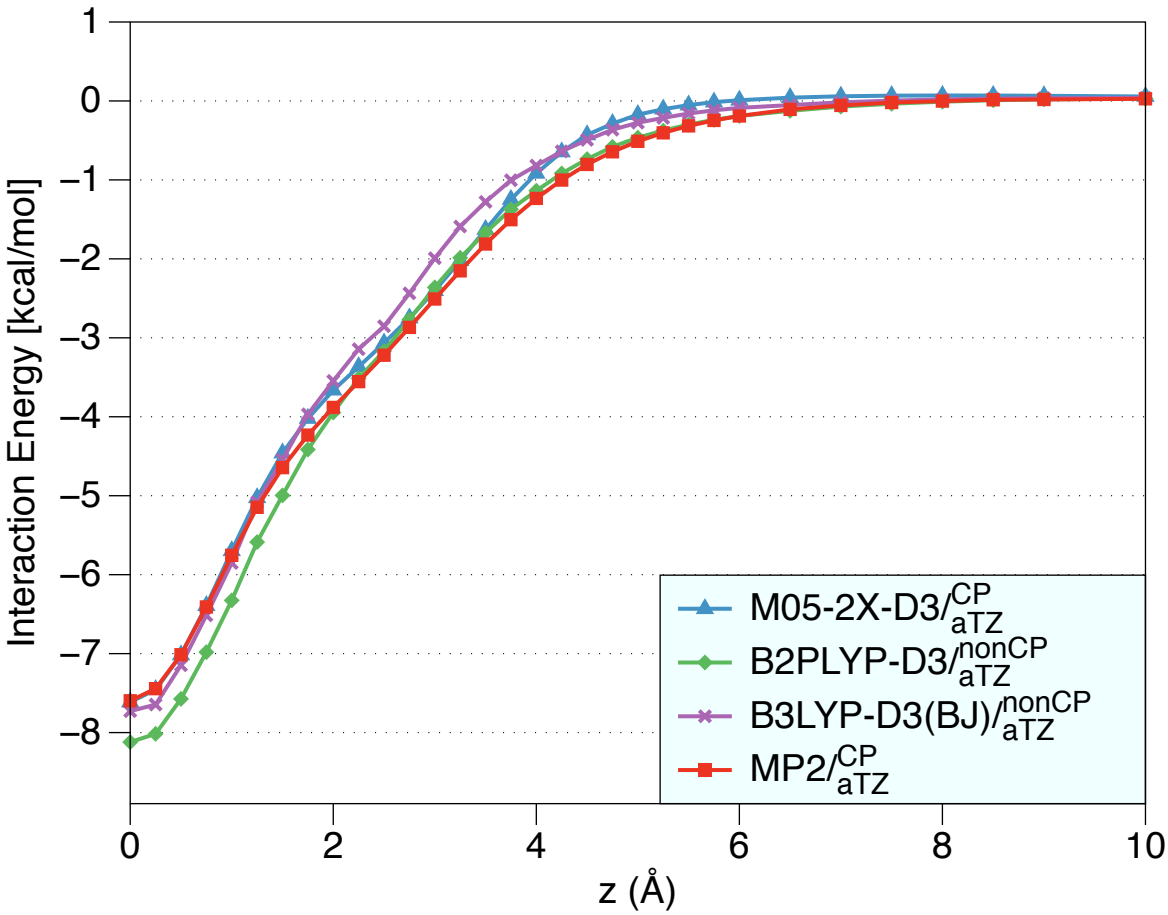

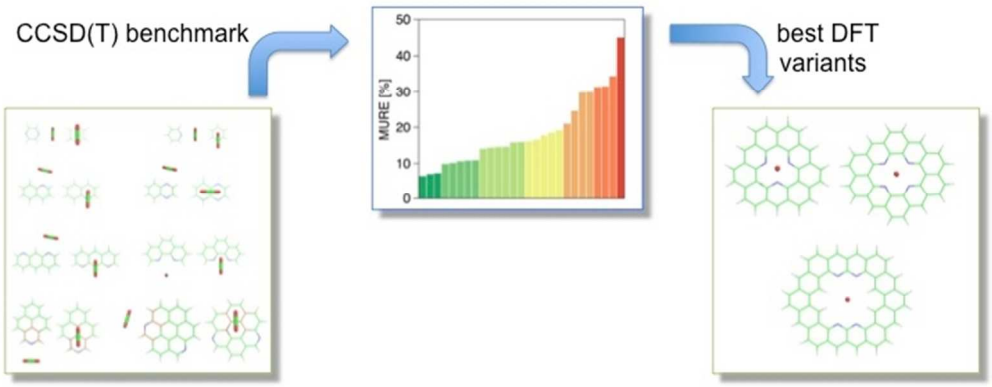

254x105mm (72 x 72 DPI)